iScience

CellPress

Article

Mechanical Regulation Underlies Effects of Exercise on Serotonin-Induced Signaling in the Prefrontal Cortex Neurons

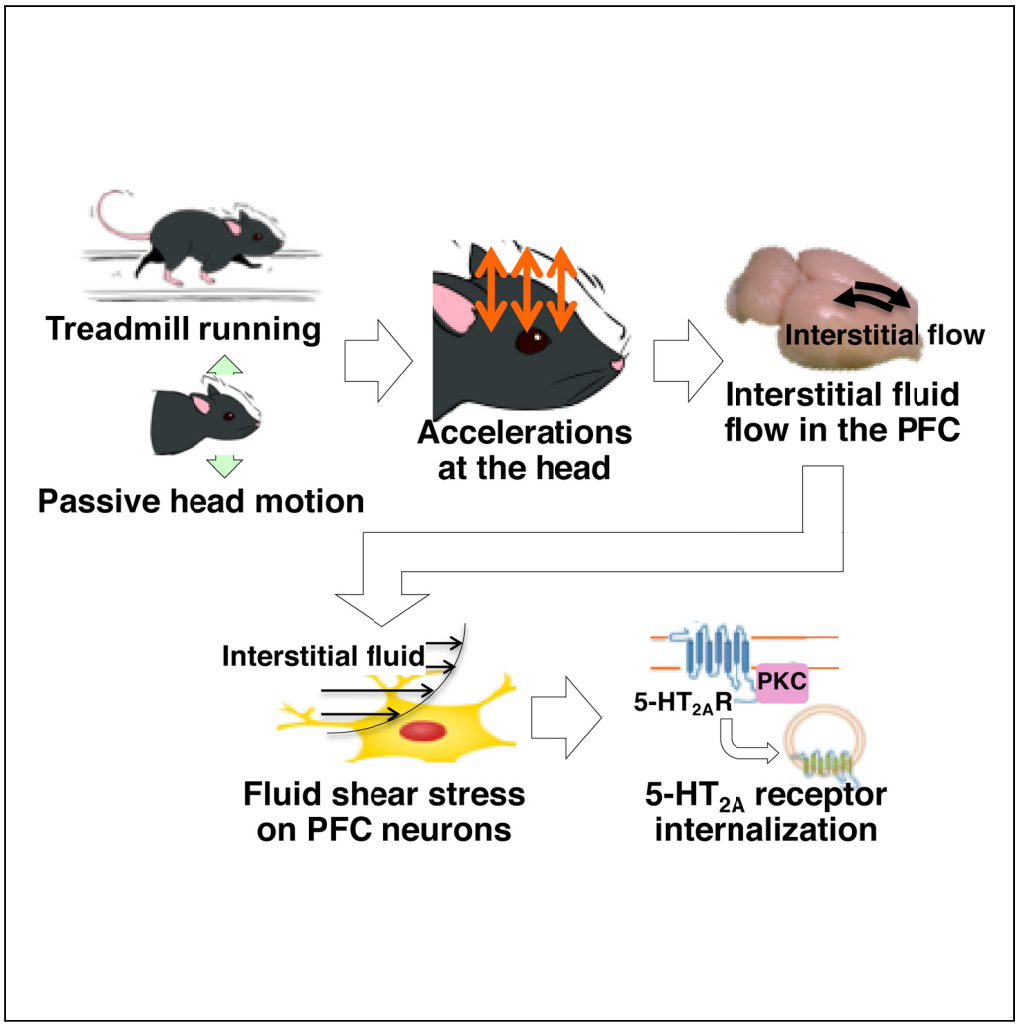

Youngjae Ryu, Takahiro Maekawa, Daisuke Yoshino, ..., Masahiro Shinohara, Motoshi Nagao, Yasuhiro Sawada

ys454-ind@umin.ac.jp

HIGHLIGHTS

Mechanical forces regulate brain functions under physiological conditions

Intracerebral interstitial fluid has mechanical roles in regulating brain functions

Mechanical impact on the head mediates effects of exercise on the brain

Fluid shear stress physiologically modulates signaling in nervous cells

Ryu et al., iScience *23*, 100874 February 21, 2020
https://doi.org/10.1016/j.isci.2020.100874

iScience

CellPress

Article

Mechanical Regulation Underlies Effects of Exercise on Serotonin-Induced Signaling in the Prefrontal Cortex Neurons

Youngjae Ryu,[1,2,11] Takahiro Maekawa,[1,11] Daisuke Yoshino,[3] Naoyoshi Sakitani,[1] Atsushi Takashima,[4] Takenobu Inoue,[4] Jun Suzurikawa,[4] Jun Toyohara,[5] Tetsuro Tago,[5] Michiru Makuuchi,[6] Naoki Fujita,[2] Keisuke Sawada,[7] Shuhei Murase,[1] Masashi Watanave,[8] Hirokazu Hirai,[8] Takamasa Sakai,[9] Yuki Yoshikawa,[9] Toru Ogata,[1] Masahiro Shinohara,[1] Motoshi Nagao,[1] and Yasuhiro Sawada[1,10,12,*]

SUMMARY

Mechanical forces are known to be involved in various biological processes. However, it remains unclear whether brain functions are mechanically regulated under physiological conditions. Here, we demonstrate that treadmill running and passive head motion (PHM), both of which produce mechanical impact on the head, have similar effects on the hallucinogenic 5-hydroxytryptamine (5-HT) receptor subtype 2A (5-HT_{2A}) signaling in the prefrontal cortex (PFC) of rodents. PHM generates interstitial fluid movement that is estimated to exert shear stress of a few pascals on cells in the PFC. Fluid shear stress of a relevant magnitude on cultured neuronal cells induces ligand-independent internalization of 5-HT_{2A} receptor, which is observed in mouse PFC neurons after treadmill running or PHM. Furthermore, inhibition of interstitial fluid movement by introducing polyethylene glycol hydrogel eliminates the effect of PHM on 5-HT_{2A} receptor signaling in the PFC. Our findings indicate that neuronal cell function can be physiologically regulated by mechanical forces in the brain.

INTRODUCTION

As the phrase "Exercise is Medicine" indicates physical exercise has been widely recognized to be effective in maintaining homeostasis of various tissues and organs. For example, aerobic exercise has been reported to be beneficial as a therapeutic intervention for cardiovascular, metabolic, and musculoskeletal disorders (Haskell et al., 2007). Exercise is also advantageous for functions of the nervous system. Therapeutic effects of exercise on numerous brain-related health problems such as dementia, schizophrenia, depression, and essential hypertension have been demonstrated (Chaar et al., 2015; Kirk-Sanchez and McGough, 2014; van Praag et al., 2014; Wang et al., 2018). However, molecular mechanisms underlying these positive effects of physical exercise on brain functions are poorly understood. Although several factors released from musculoskeletal organs, which include irisin, brain-derived neurotropic factor, and osteocalcin, are associated with the nervous system (Oury et al., 2013; Wrann, 2015), it is enigmatic whether these factors underlie the benefit of exercise with regard to brain functions. Because of this lack of adequate understanding, it is difficult to develop a scientific evidence-based guideline for exercise as a therapeutic/preventative intervention for brain-related disorders.

Among numerous biochemical signals that function in the nervous system, those related to serotonin (5-hydroxytryptamine, herein referred to as 5-HT) play essential roles in regulating emotions and behaviors and are implicated in the aforementioned psychiatric diseases (Berger et al., 2009; Canli and Lesch, 2007; Roth et al., 2004), on which exercise has been proved to have therapeutic effects. Receptors for 5-HT are expressed in various regions of the brain such as the amygdala, hippocampus, and cerebral cortex (Guiard and Di Giovanni, 2015). 5-HT receptor signaling in the prefrontal cortex (PFC), which modulates cortical neuronal activity and oscillation related to emotion and cognition (Puig and Gulledge, 2011), is implicated in psychiatric disorders (Siddiqui et al., 2008). 5-HT receptor subtypes 1A and 2A (5-HT_{1A} and 5-HT_{2A} receptors, respectively) are the two major 5-HT receptors expressed in the PFC (Puig and Gulledge, 2011). 5-HT_{1A} receptor signaling activation leads to the suppression of neuronal activity, whereas 5-HT_{2A} receptor activation provokes neuronal circuit excitability (Puig and Gulledge, 2011). Alteration in 5-HT_{2A} receptor signaling, the absence of which reduces anxiety-like behavior in mice (Weisstaub et al., 2006), is associated with many psychiatric disorders such as depression, schizophrenia, and hallucinogenic phenotypes in

[1]Department of Rehabilitation for Motor Functions, National Rehabilitation Center for Persons with Disabilities, Tokorozawa, Saitama 359-8555, Japan

[2]Department of Veterinary Surgery, Graduate School of Agricultural and Life Sciences, The University of Tokyo, Bunkyo, Tokyo 113-8657, Japan

[3]Division of Advanced Applied Physics, Institute of Engineering, Tokyo University of Agriculture and Technology, Koganei, Tokyo 184-8588, Japan

[4]Department of Assistive Technology, National Rehabilitation Center for Persons with Disabilities, Tokorozawa, Saitama 359-8555, Japan

[5]Research Team for Neuroimaging, Tokyo Metropolitan Institute of Gerontology, Itabashi, Tokyo 173-0015, Japan

[6]Section of Neuropsychology, National Rehabilitation Center for Persons with Disabilities, Tokorozawa, Saitama 359-8555, Japan

[7]University of Cincinnati College of Medicine, Cincinnati, OH 45267, USA

[8]Department of Neurophysiology & Neural Repair, Gunma University Graduate School of Medicine, Maebashi, Gunma 371-8511, Japan

[9]Department of Bioengineering, Graduate School of Engineering, The University of Tokyo, Bunkyo, Tokyo 113-8656, Japan

Continued

humans (Aghajanian and Marek, 1999; Nichols, 2004; Roth et al., 2004). Systemic administration of 2,5-dimethoxy-4-iodoamphetamine, a 5-HT_{2A} receptor agonist, enhances a depressive character, whereas pretreatment with MDL100907, a 5-HT_{2A} receptor antagonist, eliminates this effect (Diaz and Maroteaux, 2011). Treatment with D-lysergic acid diethylamide, which possesses hallucinogenic potential through massive activation of 5-HT_{2A} receptor signaling in the PFC (Egan et al., 1998), is used as a pharmacological model of psychosis in both human and animal studies (Marek and Aghajanian, 1996; Preller et al., 2018). In contrast to these negative aspects, pharmacological activation of 5-HT_{2A} receptor signaling also positively regulates cognitive functions such as learning and memory. In mice, (4-bromo-3,6-dimethoxybenzocyclobuten-1-yl)methylamine hydrobromide (TCB-2), a selective 5-HT_{2A} receptor agonist, enhances consolidation of object memory when it is administered systemically during a behavioral test for working memory (Zhang et al., 2013). Collectively, 5-HT_{2A} receptor signaling in the PFC supports normal cognitive functions; however, it can mediate emotional or psychotic disorders when it is excessively or aberrantly activated.

Many of physical exercise procedures, particularly aerobic exercises, generate mechanical loads on the head. Signaling of angiotensin II type I receptor, a member of the G-protein-coupled receptor (GPCR) family, is modified ligand independently by mechanical stress (Zou et al., 2004). Although we previously reported that treadmill running caused changes in the distribution and activity of 5-HT_{2A} receptor, another GPCR family member, in spinal cord neurons of rats (Ryu et al., 2018), it remains elusive how exercise modulates 5-HT_{2A} receptor signaling in the nervous system. Because the activity of 5-HT_{2A} receptor is modulated by its internalization, either ligand dependently or ligand independently (Bhattacharyya et al., 2002), we hypothesized that 5-HT_{2A} receptor signaling in the brain might be mechanically regulated by the receptor internalization.

RESULTS

Both Treadmill Running and Passive Head Motion Alleviate 5-HT Receptor Signaling in the Brain

We first examined whether treadmill running at a modest velocity (~10 m/min for mice and ~20 m/min for rats), a typical experimental intervention to test effects of physical exercise in rodents (Kim et al., 2010; Li et al., 2013), modulated 5-HT_{2A} receptor signaling in the brain. To this end, we quantitatively analyzed the head-twitch response (HTR), a hallucinogenic behavioral reaction that represents 5-HT_{2A} receptor activation in the PFC neurons of rodents (Canal and Morgan, 2012; Halberstadt and Geyer, 2013), induced by administration of 5-hydroxytryptophan (5-HTP), the precursor to 5-HT (Figures S1A and S1B). We found that a week of treadmill running of mice (10 m/min, 30 min per day; see Figure 1A) significantly decreased HTR (Figures 1B and 1C), representing a suppressive effect of exercise on 5-HT_{2A} receptor activation in the PFC neurons. Based on our hypothesis that gravity-derived mechanical perturbations on the brain might underpin the effects of physical exercise, we first measured the acceleration generated at the head during treadmill running. Although we examined mouse HTR because of the ease and reliability of quantitative analysis due to frequent and immediate head twitching of mice after 5-HTP administration (Bedard and Pycock, 1977; Goodwin and Green, 1985), we used rats to analyze mechanical elements related to this study. This was because the larger body size of rats enabled us to utilize various experimental tools required for analysis of physical matters and factors. We observed that the peak magnitude of the vertical acceleration generated at the rats' heads (*z* axis in Figure S1C) during treadmill running (20 m/min) was ~1.0 × *g* (Figures S1D and S1E). We therefore set up our custom-designed "passive head motion" (hereafter referred to as PHM) system to produce 1.0 × *g* of vertical acceleration peaks at the heads of rodents (mice and rats) to be tested (Figures S1D and S1E). Application of PHM to mice under isoflurane anesthesia (2 Hz, 30 min per day, 7 days; see Figure 1D) led to a decrease in HTR, similar to that after treadmill running (compare Figures 1B and 1C with Figures 1E and 1F). Mice that underwent PHM exhibited neither apparent alert problems nor detrimental consequences on behavioral activity. Collectively, we conclude that PHM and treadmill running have a comparable effect on 5-HT_{2A} receptor signaling in the PFC of rodents.

We then examined how treadmill running and PHM modulated 5-HT_{2A} receptor signaling in mouse PFC neurons. To do so, we conducted immunostaining of brain tissue sections. We observed an increase in c-Fos expression, which is downstream of 5-HT_{2A} receptor activation (Gonzalez-Maeso et al., 2007), in PFC neurons of mice after 5-HTP injection when compared with those of vehicle (saline)-injected control mice (compare top two images in Figure 1G and columns 1 and 2 in Figure 1H). Consistent with the suppressive effect of daily treadmill running or PHM (daily 30 min, 7 days) on HTR (Figures 1A–1F), both interventions down-regulated

[10]Department of Clinical Research, National Rehabilitation Center for Persons with Disabilities, Tokorozawa, Saitama 359-8555, Japan

[11]These authors contributed equally

[12]Lead contact

*Correspondence: ys454-ind@umin.ac.jp

https://doi.org/10.1016/j.isci.2020.100874

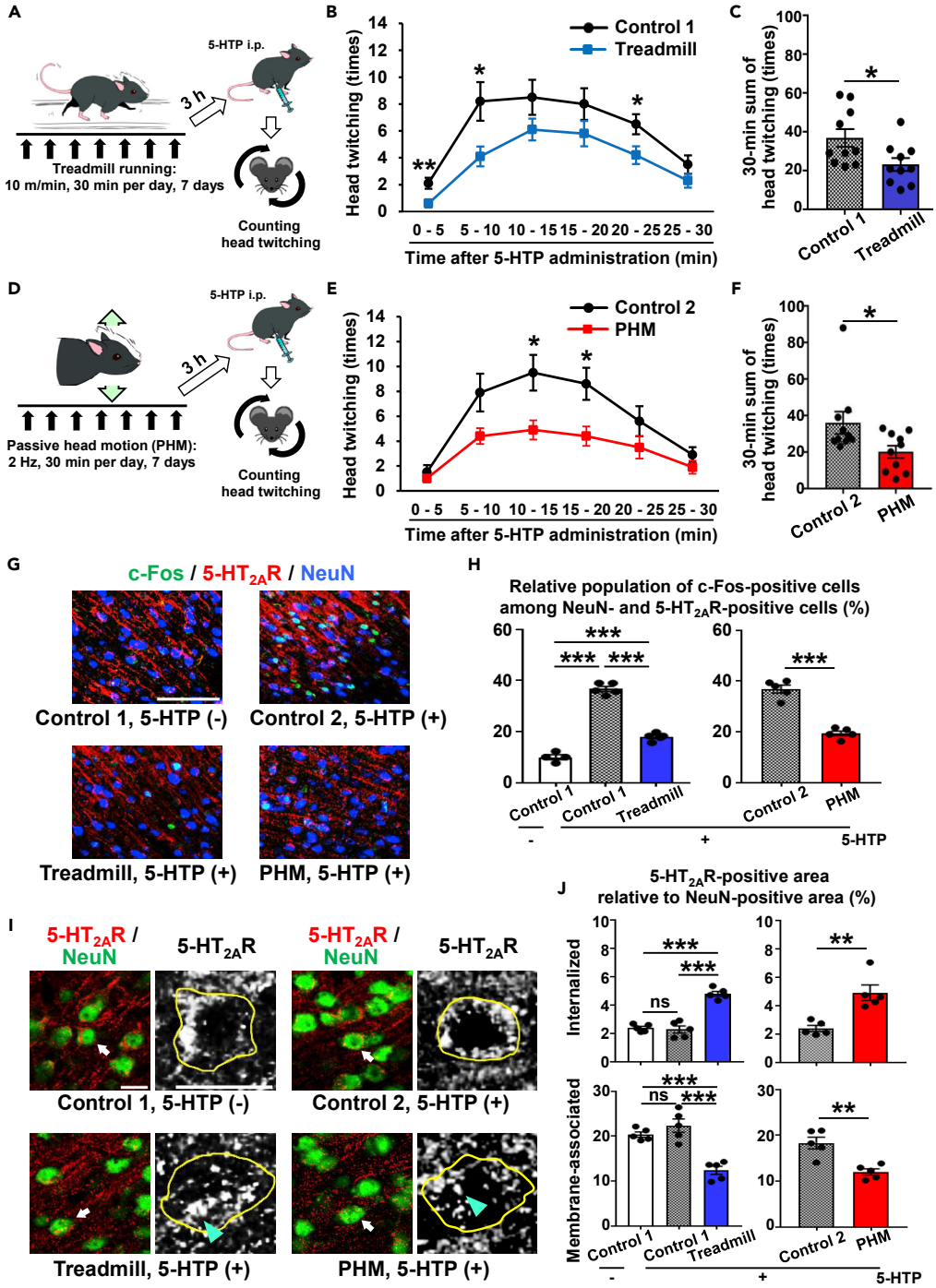

Figure 1. Treadmill Running and Passive Head Motion (PHM) Similarly Modulate Behavioral and Neuronal Response to 5-HT

(A) Schematic representation of experimental protocol for analysis of the effects of treadmill running on head-twitch response (HTR).

(B and C) Treadmill running alleviated 5-HTP-induced HTR. Count of head twitching in 5-min blocks (B) and for 30 min (C) post-5-HTP administration ($p = 0.027$, unpaired t test; $n = 10$ mice for each group). Control 1 in (B, C, G, H, I, and J) represents mice that were placed in the treadmill machine without turning it on (30 min per day, 7 days).

(D) Schematic representation of experimental protocol for analysis of the effects of PHM on HTR. PHM (cyclical 5-mm head drop) was applied to generate vertical accelerations of 1.0 × *g* peaks at the heads of mice (2 Hz, 30 min per day, 7 days).

Figure 1. *Continued*

(E and F) PHM alleviated 5-HTP-induced HTR. Head twitching was counted as in (B) and (C), respectively ($p = 0.035$, unpaired t test; $n = 10$ mice for each group). Control 2 in (E–J) represents mice that were anesthetized and placed in a prone position with their heads on the platform that was left unoscillated (30 min/day, 7 days).

(G) Micrographic images of anti-c-Fos (green), anti-5-HT_{2A} receptor (red), and anti-NeuN (blue) immunostaining of the PFC of mice administered 5-HTP (or vehicle) after a week of daily treadmill running or PHM. Scale bar, 100 μm. Images are representative of four to five mice.

(H) Both treadmill running and PHM decreased c-Fos expression in 5-HT_{2A} receptor-positive neurons of mouse PFC. Relative population (%) of c-Fos-positive cells of 300 NeuN- and 5-HT_{2A} receptor-positive cells is shown (left chart: $p < 0.001$, one-way ANOVA with post hoc Bonferroni test; right chart: $p < 0.001$, unpaired t test; $n = 4$ mice for columns 1, $n = 5$ mice for columns 2 to 5).

(I) Micrographic images of anti-5-HT_{2A} receptor (5-HT_{2A}R; red) and anti-NeuN (green) immunostaining of the PFC of mice injected with 5-HTP (or vehicle) after a week of daily treadmill running or PHM. Higher-magnification images of anti-5-HT_{2A} receptor immunostaining of arrow-pointed cells are presented with a gray scale. Yellow lines indicate the margins of somas outlined by NeuN-positive signals, and cyan arrowheads point to internalized anti-5-HT_{2A} receptor immunosignals. Scale bars, 20 μm. Images are representative of five mice.

(J) Quantification of internalized and membrane-associated 5-HT_{2A} receptor-positive area relative to NeuN-positive area in mouse PFC. Thirty-five to forty NeuN-positive neuronal somas were analyzed for each mouse (Internalized: left chart, $p < 0.001$, one-way ANOVA with post hoc Bonferroni test; right chart, $p = 0.0027$, unpaired t test; Membrane-associated: left chart, $p < 0.001$, one-way ANOVA with post hoc Bonferroni test; right chart, $p = 0.0025$, unpaired t test; $n = 5$ mice for each group). Data for 5-HTP(+) samples in (G–J) were obtained from mice infused with 4% paraformaldehyde/PBS immediately after HTR test shown in (B, C, E, and F).

Data are represented as means ± SEM. *$p < 0.05$, **$p < 0.01$, ***$p < 0.001$; ns, not significant. See also Figures S1, S2, S3, and S4.

5-HTP-induced c-Fos expression in the PFC neurons (bottom two images in Figure 1G, and compare columns 2 versus 3 and 4 versus 5 in Figure 1H). Notably, our quantitative analysis of 5-HT_{2A} receptor distribution in neuronal cells (Figures S2A–S2D; see Methods) revealed that both treadmill running and PHM significantly increased 5-HT_{2A} receptor internalization in mouse PFC neurons (Figures 1I and 1J). In contrast, the expression of 5-HT_{2A} receptor (mRNA and protein) in mouse PFC was not significantly changed by treadmill running or PHM (Figures S2E and S2F). Considering that 5-HT_{2A} receptor expression is highly neuron specific in rodent cerebral cortex (Cornea-Hebert et al., 1999), neither treadmill running nor PHM appears to significantly alter 5-HT_{2A} receptor expression in the PFC neurons. These findings suggest that 5-HT_{2A} receptor internalization, rather than decreased expression, is involved in the suppression of 5-HT_{2A} receptor signaling in PFC neurons by treadmill running or PHM.

Both suppression of HTR and 5-HT_{2A} receptor internalization in the PFC neurons were observed even 72 h after the last bout of 1-week daily treadmill running of mice (10 m/min, 30 min per day) (Figures S3A–S3E). In contrast, neither of them was significant 7 days after the last treadmill running (Figures S3F–S3J). Furthermore, the effects of 1-week daily PHM (2 Hz, 30 min per day) on HTR and 5-HT_{2A} receptor internalization in the PFC neurons were observed 72 h (Figures S4A–S4E), but not 7 days (Figures S4F–S4J), after its last bout. These results indicate that the effects of 1-week daily treadmill running or PHM last longer than 72 h, but shorter than 7 days. The apparent consistency between the longer-term effects of treadmill running and PHM (compare Figures S3 and S4) agrees with the mechanistic correlation between HTR suppression and 5-HT_{2A} receptor internalization in the PFC neurons and supports the relevance of PHM to treadmill running.

PHM Generates Low-Amplitude Intracerebral Pressure Waves and Induces Interstitial Fluid Flow in the PFC

Although vigorous deformations such as stretching of neurons likely have damaging effects (e.g., brain contusion or traumatic brain injury), the brain is not a rigid organ. Therefore, minimal deforming forces or stress distribution changes are possibly produced in the brain under physiological conditions. To analyze the physical effects that PHM produced in the brains of rodents, we measured the local pressure in rats' PFC using a telemetry pressure sensor (Figure 2A). We found that PHM generated pressure waves (changes) with ~1 mm Hg peak amplitude (Figures 2B–2D). Hydrostatic pressure of this magnitude (~1.3 cmH_2O) is unlikely to initiate mechanosensing signaling in cells (Tworkoski et al., 2018). Assuming an analogy with osteocytes embedded in bones, the function of which is known to be modulated by interstitial fluid flow-derived shear stress (Klein-Nulend et al., 2013), we speculated that minimal stress distribution changes might generate interstitial fluid flow in the brain, resulting in shear stress-mediated regulation of neuronal functions.

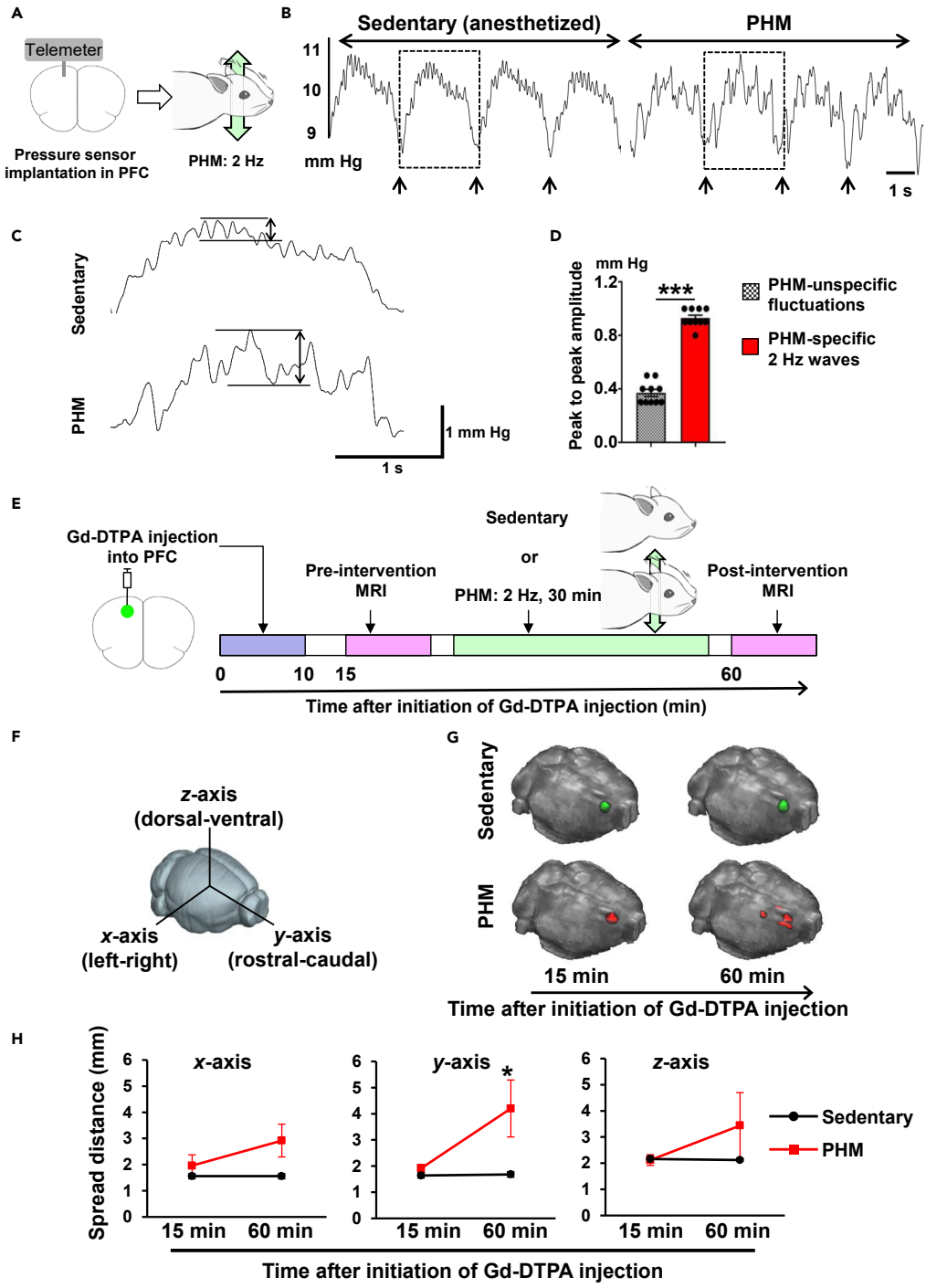

Figure 2. PHM Generates Intracerebral Pressure (ICP) Waves of Low Amplitude, but Facilitates Cerebral Interstitial Fluid Movement (Flow) in the PFC

(A–D) PHM generated ~1 mm Hg ICP changes. (A) Schematic representation of ICP measurement at rats' PFC. (B) Representative ICP waves recorded in rats' PFC during sedentary condition and PHM. Arrows indicate the time points of transition from inhalation to exhalation detected by simultaneous respiration monitoring. Scale bar, 1 s. Images are representative of two independent experiments with similar results. (C) Respiration-unsynchronized ICP changes. Respiration-synchronized ICP waves indicated by rectangles in (B) are presented with higher magnification. Right-angled scale bar, 1 s/1 mm Hg. Note that 2-Hz ICP waves indicated by a two-headed arrow were specifically generated during PHM. (D) Magnitude of PHM-specific and PHM-unspecific ICP changes unsynchronized with respiration. Peak-to-peak

Figure 2. *Continued*

magnitudes indicated by two-headed arrows in (C) were quantified. Data are represented as means ± SEM. ***p < 0.001 (unpaired t test, 10 segments analyzed for each).

(E–H) PHM facilitates cerebral interstitial fluid movement (flow). (E) Schematic representation of experimental protocol for magnetic resonance imaging analysis of Gd-DTPA injected in rats' PFC. (F) Definition of x (left-right), y (rostral-caudal), and z (dorsal-ventral) axes used in this study. (G) Representative Gd-DTPA spreading presented on a surface-rendered brain. Gd-DTPA clusters are indicated by green (sedentary) and red (PHM). Images are representative of five rats. (H) Quantification of Gd-DTPA spreading along each axis. Red line: PHM (n = 5), black line: sedentary (n = 5). Data are represented as means ± SEM. *p < 0.05 (x axis: p = 0.065, y axis: p = 0.049, z axis: p = 0.33, unpaired t test).

See also Figures S5 and S6, and Table S1.

To measure the PHM-induced interstitial fluid movement in the brain, we injected gadolinium-diethylenetriamine pentaacetic acid (Gd-DTPA), an extracellular fluid contrast agent, into the PFC of anesthetized rats (Figure 2E) and tracked its distribution with magnetic resonance imaging (Figures S5A and S5B). We found that PHM significantly promoted Gd-DTPA spreading in the rostral-caudal (*y* axis, Figure 2F) direction (Figures 2G and 2H). In contrast, PHM did not significantly affect the left-right and dorsal-ventral spreading (x and z axes, Figure 2F) of Gd-DTPA (Figures 2G and 2H), suggesting that PHM may enhance interstitial fluid flow in the PFC in a defined direction, rather than isotropically. Our simulative calculation suggests that PHM subjected PFC neurons to interstitial fluid flow-derived shear stress with an average magnitude of 0.86–3.9 Pa (Table S1). Fluid shear stress (FSS) of this magnitude is known to modify the physiological function of astrocytes (Maneshi et al., 2017), the most abundant type of cells distributed in the brain.

Based on our observation of anisotropic movement of intracerebral interstitial fluid induced by PHM (Figures 2G and 2H), we tested PHM in the directions other than the vertical one. One-week daily PHM (30 min per day) in the left-right direction (Figure S6A, top), which selectively produced 1.0 × *g* of x axis acceleration peaks at rodents' heads (Figures S1C and S6A, bottom), suppressed HTR (Figures S6B and S6C) and induced 5-HT_{2A} receptor internalization in the PFC neurons (Figures S6D and S6E) of mice. In contrast, PHM in the rostral-caudal direction (Figure S6F, top), which produced 1.0 × *g* of y axis acceleration peaks (Figures S1C and S6F, bottom), neither decreased HTR nor induced 5-HT_{2A} receptor internalization in the PFC neurons of mice (Figures S6G-S6J). These results may relate to the directional selectivity (or anisotropy) in intracerebral interstitial fluid movement (Figures 2G and 2H) and agree with the mechanistic correlation between PHM-induced suppression of HTR and 5-HT_{2A} receptor internalization in the PFC neurons of mice.

FSS on Neuronal Cells Induces 5-HT_{2A} Receptor Internalization

5-HT_{2A} receptor internalization was commonly observed in PFC neurons of mice after treadmill running and PHM (Figures 1I, 1J, S3D, S3E, S4D, S4E, S6D and S6E). Therefore, we postulated a common regulatory mechanism underlying this internalization and hypothesized that 5-HT_{2A} receptor might be internalized in PFC neurons as a cellular response to mechanical forces generated by the cyclical accelerations with 1.0 × *g* peaks (Figures S1D, S1E and S6A, bottom). To test this hypothesis, we conducted *in vitro* experiments to examine whether 5-HT_{2A} receptor expressed in cultured neuronal cells was internalized in response to FSS. Based on our simulation mentioned above, we applied pulsatile FSS with an average magnitude of 0.91 Pa to Neuro2A cells, which exhibit neuronal phenotypes and morphology (Goshima et al., 1993; Yun et al., 2013), using a system we previously reported (Yoshino et al., 2013). Similar to what was observed after 5-HT administration, FSS application (0.91 Pa, 0.5 Hz, 30 min) caused internalization of 5-HT_{2A} receptors expressed in Neuro2A cells (Figure 3A). However, FSS-induced 5-HT_{2A} receptor internalization appeared different from that after 5-HT administration. As shown in Figures 3B and 3C, 5-HT_{2A} receptor internalization increased incrementally up to 3 h after cessation of FSS (3.5 h after initiation of FSS), whereas it became insignificant 3 h after 5-HT administration. Notably, 5-HT_{2A} receptor internalization remained significantly enhanced even 24 h after FSS application (Figure 3C).

The short duration of ligand-dependent (i.e., 5-HT-induced) 5-HT_{2A} receptor internalization in Neuro2A cells is consistent with the lack of significant changes regarding 5-HT_{2A} receptor internalization in the PFC neurons between mice with and without 5-HTP injection that was carried out >30 min before the transcardial paraformaldehyde infusion (compare columns 1 and 2 in Figure 1J). These findings suggest that the mechanisms of 5-HT_{2A} receptor shuttling/recycling are at least partially distinct between post-FSS application and post-5-HT administration.

Consistent with the 5-HT_{2A} receptor internalization, we observed via immunostaining analysis that FSS alleviated 5-HT-induced phosphorylation of extracellular signal-regulated kinase (ERK) (Figure 3D) and

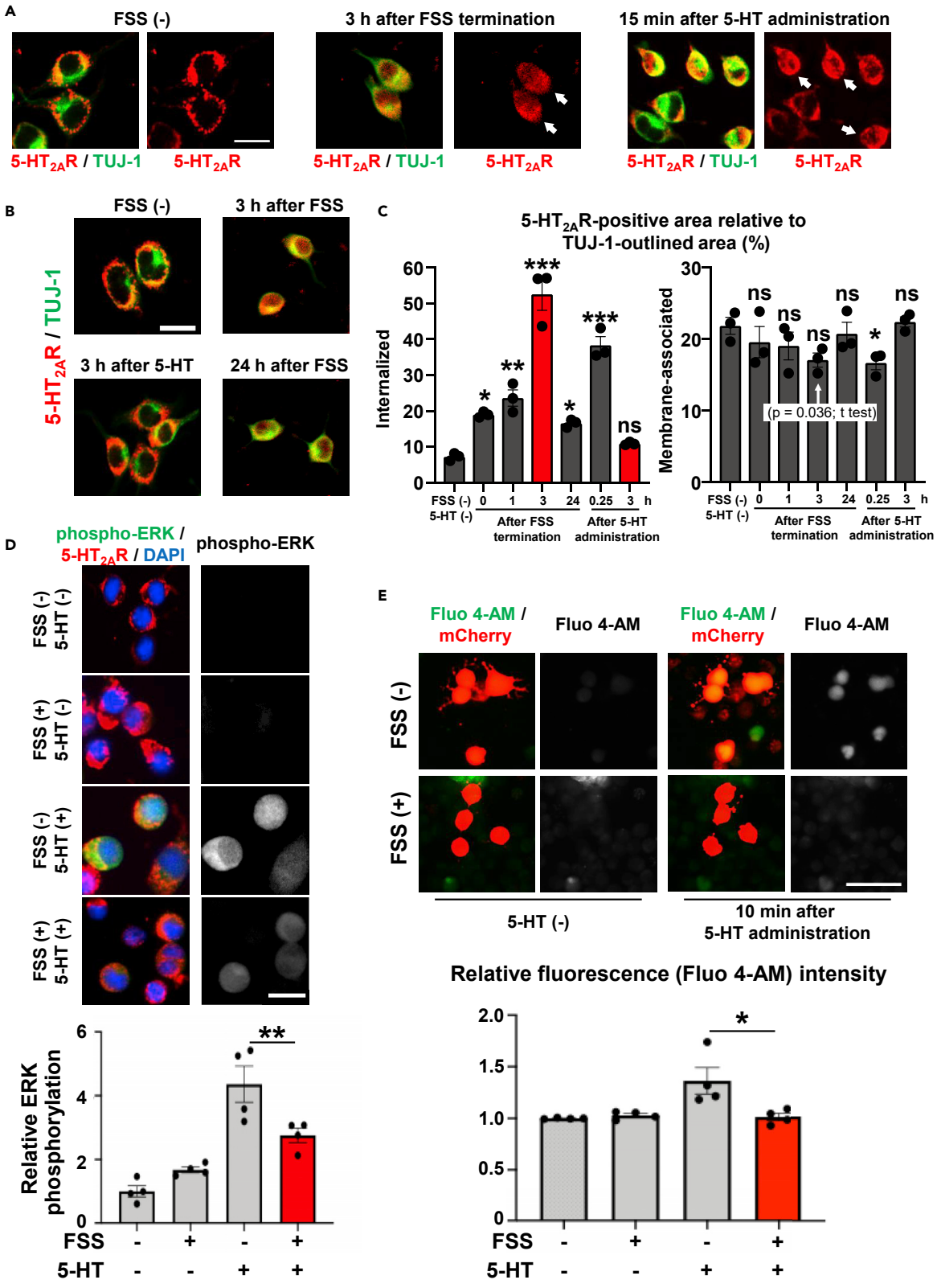
A
FSS (-)
3 h after FSS termination
15 min after 5-HT administration
5-HT2AR / TUJ-1
5-HT2AR
B
FSS (-)
3 h after FSS
3 h after 5-HT
24 h after FSS
5-HT2AR / TUJ-1
C
5-HT2AR-positive area relative to TUJ-1-outlined area (%)
Internalized
Membrane-associated
(p = 0.036; t test)
FSS (-) 5-HT (-)
After FSS termination
After 5-HT administration
D
phospho-ERK / 5-HT2AR / DAPI
phospho-ERK
FSS (-) 5-HT (-)
FSS (+) 5-HT (-)
FSS (-) 5-HT (+)
FSS (+) 5-HT (+)
Relative ERK phosphorylation
FSS
5-HT
E
Fluo 4-AM / mCherry
Fluo 4-AM
FSS (-)
FSS (+)
5-HT (-)
10 min after 5-HT administration
Relative fluorescence (Fluo 4-AM) intensity

Figure 3. Fluid Shear Stress (FSS) Internalizes 5-HT$_{2A}$ Receptor Expressed in Neuro2A Cells and Modulates Their Responses to 5-HT

(A) 5-HT$_{2A}$ receptor was internalized after FSS. Neuro2A cells grown in a poly-D-lysine-coated dish were subjected to pulsatile FSS (average 0.91 Pa, 0.5 Hz, 30 min) or treated with 5-HT (10 μM), fixed, and stained for 5-HT$_{2A}$ receptor (5-HT$_{2A}$R; red). To define their soma outlines, co-immunostaining of TUJ-1 was conducted (green). Left, control; middle, 3 h after the termination of FSS; right, 15 min after 5-HT administration. Arrows point to cells with apparent 5-HT$_{2A}$ receptor internalization. Scale bar, 20 μm. Images are representative of three independent experiments with similar results.

(B and C) 5-HT$_{2A}$ receptor internalization lasted longer after FSS, when compared with after 5-HT administration. (B) Micrographic images of Neuro2A cells, with and without FSS application, stained for 5-HT$_{2A}$ receptor (5-HT$_{2A}$R; red) and TUJ-1 (green). Scale bar, 20 μm. Images are representative of three independent experiments with similar results. (C) Quantification of internalized and membrane-associated 5-HT$_{2A}$ receptor-positive area relative to TUJ-1-outlined area in Neuro2A cells. Internalized and membrane-associated 5-HT$_{2A}$ receptor-positive immunosignals were defined as in Figure S2D and quantified as in Figure 1J (left chart: FSS, $p < 0.0001$ for ANOVA, $p = 0.014$ for 0 h, $p = 0.0016$ for 1 h, $p < 0.0001$ for 3 h, $p = 0.049$ for 24 h. 5-HT, $p < 0.0001$ for ANOVA, $p < 0.0001$ for 0.25 h, $p = 0.20$ for 3 h. Right chart: FSS, $p = 0.36$ for ANOVA, $p = 0.73$ for 0 h, $p = 0.58$ for 1 h, $p = 0.19$ for 3 h, $p = 0.97$ for 24 h. 5-HT, $p = 0.010$ for ANOVA, $p = 0.016$ for 0.25 h, $p = 0.89$ for 3 h, one-way ANOVA with post hoc Dunnett's test; 20 cells analyzed in each sample, n = 3 for each group).

(D) FSS alleviated 5-HT-induced ERK phosphorylation in neuronal cells. Neuro2A cells were either left unexposed or exposed to pulsatile FSS (average 0.91 Pa, 0.5 Hz, 30 min). Three hours after FSS termination, cells were treated with 5-HT (10 μM) for 15 min, fixed and stained for 5-HT$_{2A}$ receptor (5-HT$_{2A}$R; red), phospho-ERK (green), and DAPI (blue). Top, micrographic images. Scale bar, 25 μm. Bottom, Quantification of anti-phospho-ERK immuno-intensity: signal intensity of anti-phospho-ERK immunostaining was quantified using "auto-threshold" of ImageJ, and immuno-intensity was calculated by referring the cumulated intensity values to the total positive signal area and scaled with the mean of the control sample (FSS-, 5-HT-) set at 1 ($p = 0.0058$, one-way ANOVA with post hoc Bonferroni test, 50 cells analyzed in each sample, n = 4 for each group).

(E) FSS attenuated 5-HT-induced increase in intracellular Ca^{2+} concentration. Neuro2A cells were either left unexposed or exposed to FSS (average 0.91 Pa, 0.5 Hz, 30 min). Three hours after the termination of FSS, cells were treated with 5-HT (10 μM) for 10 min and subjected to measurement of intracellular Ca^{2+} concentration using Fluo 4-AM as described in Methods. Top, micrographic images. Scale bar, 50 μm. Bottom, intracellular Ca^{2+} concentration represented as relative fluorescence intensity with the mean fluorescence value from cells before 5-HT administration set as 1 ($p = 0.0138$, one-way ANOVA with post hoc Bonferroni test; 50 cells analyzed in each sample, n = 4 for each group).

Data are represented as means ± SEM. *$p < 0.05$, **$p < 0.01$, ***$p < 0.001$; ns, not significant. See also Figure S2.

increase in intracellular Ca^{2+} concentration (Figure 3E) in Neuro2A cells. Collectively, these results indicate that FSS desensitizes Neuro2A cells to 5-HT by inducing prolonged 5-HT$_{2A}$ receptor internalization.

PKCγ Is Responsible for FSS-Induced 5-HT$_{2A}$ Receptor Internalization in Neuro2A Cells

We next looked into whether FSS-induced desensitization of Neuro2A cells to 5-HT was relevant to the attenuation of HTR by PHM. It has been reported that HTR is up-regulated in mice that are genetically defective in protein kinase Cγ (PKCγ) (Bowers et al., 2006), the major PKC subtype expressed in neuronal cells (Saito and Shirai, 2002). Furthermore, PKC, which can be activated by FSS (Kroll et al., 1993), is involved in GPCR internalization in various types of cells (Chapell et al., 1998; Liles et al., 1986; Park et al., 2009). We therefore examined whether PKCγ was involved in 5-HT$_{2A}$ receptor internalization after the application of FSS *in vitro*. Our immunostaining analysis of Neuro2A cells revealed that FSS enhanced phosphorylation of myristoylated alanine-rich protein kinase C substrate (MARCKS), a major PKC substrate (Hartwig et al., 1992) (compare top and middle rows in Figure 4A). However, FSS-induced MARCKS phosphorylation was hardly observed in Neuro2A cells pre-treated with a PKC inhibitor, Ro 31-8220 (bottom row in Figure 4A). In addition, FSS application decreased nuclear distribution of PKCγ, which relates to its activation in cultured neuronal cells (Menard et al., 2013) (Figure 4B). Furthermore, PKC inhibition significantly attenuated 5-HT$_{2A}$ receptor internalization in Neuro2A cells after 5-HT administration or FSS application (Figures 4C and 4D). These results suggest that PKC activation is responsible for FSS-induced desensitization of Neuro2A cells to 5-HT.

Administration of a PKC Inhibitor Eliminates the PHM Effects on the PFC Neurons

We then tested if PKC activation was involved in 5-HT$_{2A}$ receptor internalization *in vivo*, as indicated in the suppressive effect of PHM on HTR. When we injected Ro 31-8220 (5 mg/kg, intraperitoneally) before each bout of daily PHM for a week (Figure 4E), there was an increase in HTR after 5-HTP administration, nullifying the effects of PHM on HTR (Figures 4F and 4G). Histologically, the effects of PHM on c-Fos expression and 5-HT$_{2A}$ receptor internalization in the PFC neurons were significantly reduced by Ro 31-8220 pre-administration (Figure S7). All in all, we conclude that PKCγ activation is at least partly responsible for FSS-induced desensitization of Neuro2A cells to 5-HT *in vitro* as well as the suppressive effect of PHM on HTR after 5-HTP administration *in vivo*. The relatively long duration of FSS-induced 5-HT$_{2A}$ receptor internalization in Neuro2A cells (Figure 3C) poses a possibility of cumulative effects of FSS applied repeatedly. Therefore, our findings support the notion that FSS-induced desensitization of Neuro2A cells *in vitro* is relevant to the suppression of HTR by PHM *in vivo*. Mechanosensitive ion channels that are responsible for FSS-induced increase in intracellular Ca^{2+} (Hyman et al., 2017) may mediate FSS-dependent PKC activation

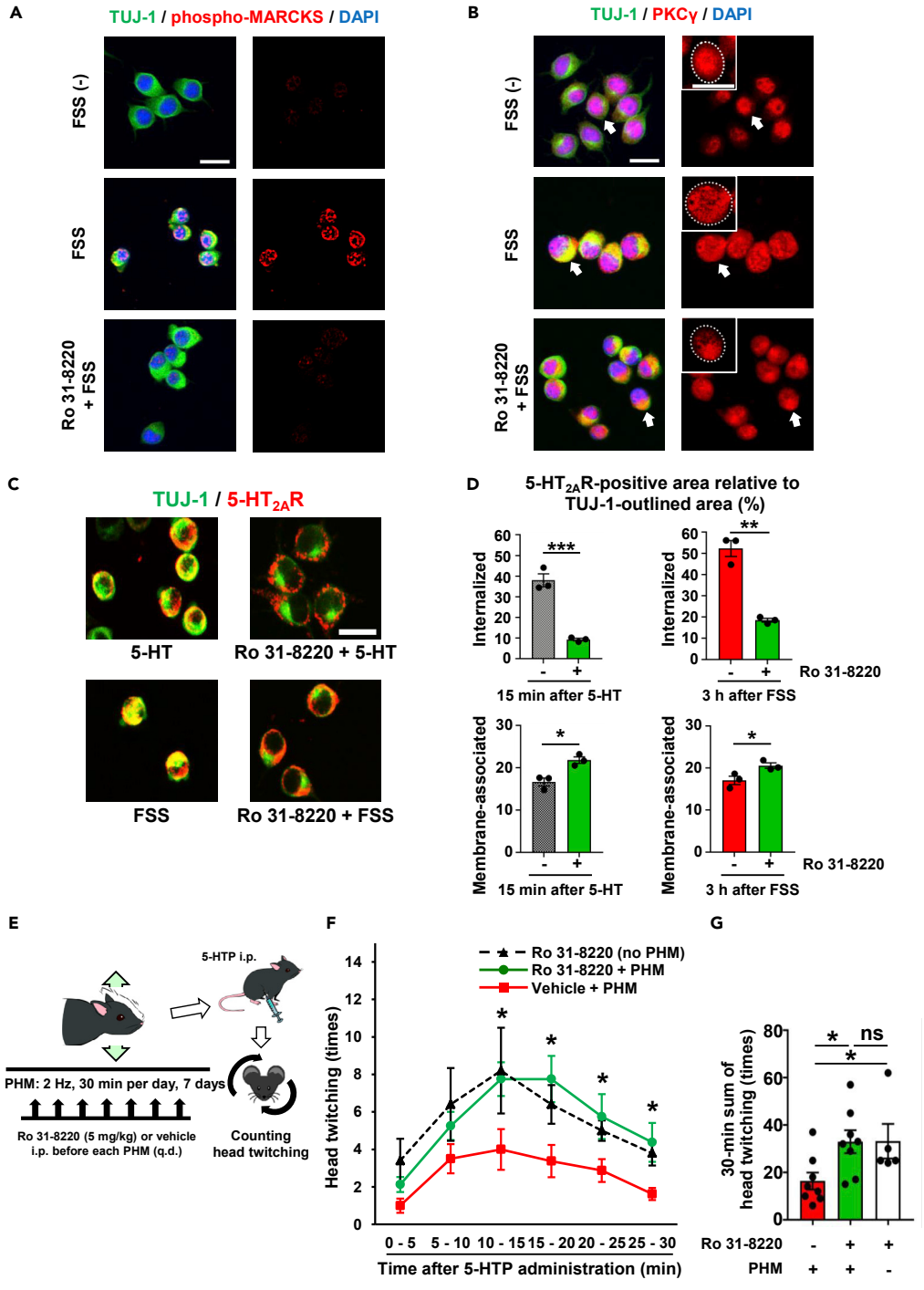

Figure 4. PKC Is Involved in Both FSS-Induced 5-HT$_{2A}$ Receptor Internalization *In Vitro* and PHM-Attenuated HTR *In Vivo*

(A and B) MARCKS was phosphorylated in neuronal cells after FSS, depending on PKC activity. Neuro2A cells, either left unexposed or exposed to FSS (average 0.91 Pa, 0.5 Hz, 30 min) with and without PKC inhibitor pretreatment (Ro 31-8220; 4 μM, 1 h), were subjected to anti-TUJ-1 (green) and anti-phospho-MARCKS (red in A) or anti-PKCγ (red in B) immunostaining. Nuclei were stained with DAPI. Higher-magnification images of anti-PKCγ immunostaining of arrow-pointed cells are presented with cell margins (white dashed lines) as insets (B). Scale bars, 20 μm. Images are representative of three independent experiments with similar results.

Figure 4. *Continued*

(C) PKC inhibition hampered both 5-HT- and FSS-induced 5-HT_{2A} receptor internalization. Neuro2A cells with combinations of Ro 31-8220 pretreatment and 5-HT administration (10 μM, 15 min) or FSS application (average 0.91 Pa, 0.5 Hz, 30 min) were fixed and stained for 5-HT_{2A} receptor (5-HT_{2A}R; red) and TUJ-1 (green). Scale bars, 20 μm. Images are representative of three independent experiments with similar results.

(D) Quantification of 5-HT_{2A} receptor internalization (top left chart: $p < 0.001$, top right chart: $p = 0.001$, bottom left chart: $p = 0.013$, bottom right chart: $p = 0.041$, unpaired t test; 20 cells analyzed in each sample, $n = 3$ for each group).

(E) Schematic representation of the experimental protocol for PHM with PKC inhibition. Ro 31-8220 or vehicle was injected just before each bout of PHM.

(F and G) PKC inhibition nullified the effect of PHM on 5-HTP-induced HTR. Head twitching was counted as in Figures 1B and 1C. (F) Count of head twitching in 5-min blocks. Asterisks (*) indicate statistical significance between PHM with (green line) and without (red line) Ro 31-8220 (10–15 min: $p = 0.019$, 15–20 min: $p = 0.012$, 20–25 min: $p = 0.049$, 25–30 min: $p = 0.024$, unpaired t test; $n = 8$ mice for each group), whereas there were no significant differences at any time point between Ro 31-8220 with (green line) and without (black line) PHM ($p > 0.05$, unpaired t test; $n = 5$ mice for group of Ro 31-8220 without PHM). (G) Total count of head twitching for 30 min after 5-HTP administration (column 1 versus 2: $p = 0.016$, column 1 versus 3: $p = 0.041$, column 2 versus 3: $p = 0.98$, unpaired t test).

Data are represented as means ± SEM. *$p < 0.05$, **$p < 0.01$, ***$p < 0.001$; ns, not significant. See also Figures S2 and S7.

(Berk et al., 1995), but the molecular events upstream of PKC activation in response to FSS remain to be determined.

PHM Neither Decreases HTR nor Increases 5-HT_{2A} Receptor Internalization when Interstitial Fluid Movement Is Hindered by Hydrogel Introduction in the PFC

To examine whether interstitial fluid movement mediated the effects of PHM on the 5-HT_{2A} receptor signaling in PFC neurons, we modulated interstitial fluid dynamics in mouse PFC and conducted PHM experiments. To this end, we gelled the interstitial fluid *in situ* and deprived its fluidity (Figures S8A–S8C) by intracerebrally injecting mutually reactive polyethylene glycol (PEG) gel precursor (pre-gel) solutions (Figure 5A), whose biocompatibility has been confirmed previously (Hayashi et al., 2017). Injection of the pre-gel solutions pre-mixed just before use rendered them spread over mouse PFC and gelled the interstitial fluid *in situ* (Figure S8A). Consistent with our previous observation that gelation only inhibits the fluidity of the fluid but does not restrict the diffusion of small molecules inside the gel (Fujiyabu et al., 2018), hydrogel introduction did not cause apparent delays in HTR after 5-HTP injection (Figure S8D), indicating the rapid access of 5-HT to PFC neurons.

Although 1-week daily PHM decreased HTR in mice injected with the control PEG solution, hydrogel introduction in the PFC eliminated this decreasing effect of PHM (Figures 5B and 5C). Hydrogel introduction alone appeared to slightly increase HTR when compared with the control PEG injection (see first HTR test, Figure 5C, right chart), whereas PHM made the difference significant (see second HTR test, Figure 5C, right chart). This is consistent with the notion that interstitial fluid movement is involved in the suppressive effect of PHM on HTR. Furthermore, hydrogel introduction eliminated the increasing effect of PHM on 5-HT_{2A} receptor internalization in mouse PFC neurons (Figures 5D and 5E). In addition to the aforementioned rapid solute diffusivity through the hydrogels, the expression level of 5-HT_{2A} receptor (Figures S8E and S8F), neuronal survival and apoptosis (Figures S8G and S8H), and overall cell apoptosis (Figure S8I) in mouse PFC were not altered by hydrogel introduction. Therefore it is unlikely that the increasing effects of hydrogel introduction on HTR and membrane association of 5-HT_{2A} receptor resulted from decreased cell viability caused by impaired nutrient supply or removal of metabolic wastes. Collectively, hydrogel introduction in mouse PFC appears to eliminate PHM effects by hindering interstitial fluid movement, indicating the relevance of FSS-induced desensitization of Neuro2A cells to 5-HT *in vitro* to the suppression of HTR by PHM *in vivo*.

DISCUSSION

Here, we demonstrate that mechanical perturbation that reproduces mechanical impact on the head during walking or light jogging modulates 5-HT_{2A} receptor signaling in the PFC of rodents. Many aerobic exercises, including walking and running, involve impact-generating bodily actions creating sharp accelerations at the head upon foot contacting with the ground. Therefore, their beneficial effects as therapeutic/preventative procedures for a variety of diseases and health disorders may rely at least partly on modest changes in mechanical stress distribution in the brain, which may prompt optimal FSS on cerebral neurons. It is possible that such mechanical impact concomitant with walking/running underlies positive effects of

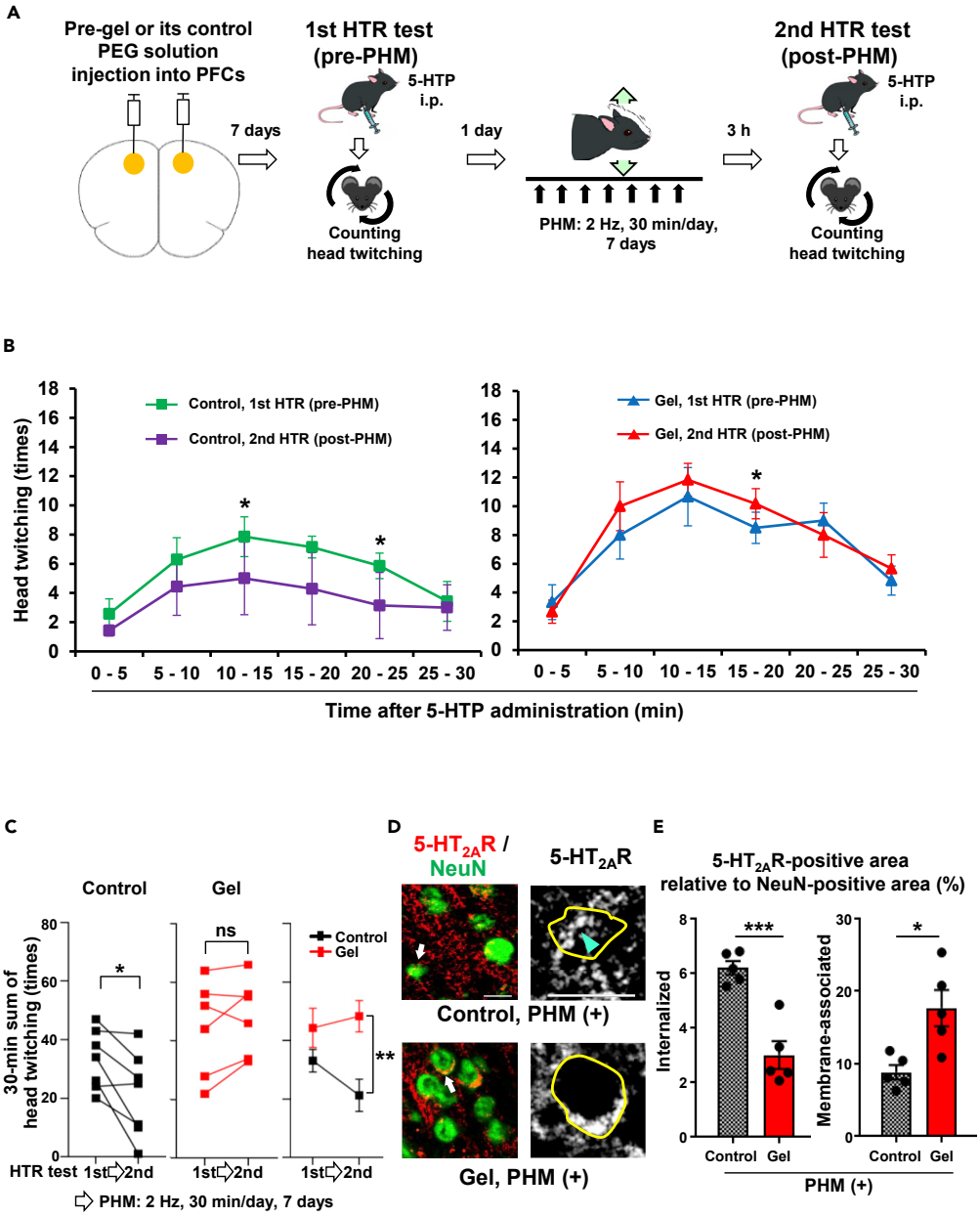

Figure 5. Hydrogel Introduction Modulates Interstitial Fluid Movement and Eliminates Suppressive Effects of PHM on 5-HT$_{2A}$ Receptor Signaling in Mouse PFC Neurons

(A) Schematic representation of experimental protocol for analysis of the effects of PHM on HTR with and without PEG hydrogel introduction in mice PFC. PHM was applied daily for 7 days between the first and the second HTR tests.

(B and C) Hydrogel introduction in the PFC eliminates the decreasing effects of PHM on HTR. Head twitching was counted as in Figures 1B and 1C (n = 7 mice for control group, n = 6 mice for Gel group). (B) Count of head twitching in 5-min blocks after 5-HTP administration to mice injected with control (left chart, 10–15 min: $p = 0.035$, 20–25 min: $p = 0.042$, paired t test) or pre-gel PEG solution (right chart, 15–20 min: $p = 0.042$, paired t test). (C) Results of the first and second HTR tests are shown by total count of head twitching for 30 min after 5-HTP administration: individual mice (left chart: $p = 0.021$, center chart: $p = 0.22$, paired t test) and each group (right chart, first HTR: $p = 0.15$, second HTR: $p = 0.0017$, two-way ANOVA with post hoc Bonferroni test).

(D) Micrographic images of anti-5-HT$_{2A}$ receptor (5-HT$_{2A}$R; red) and anti-NeuN (green) immunostaining of PFC, either with or without hydrogel introduction, of mice subjected to PHM. Histological samples of the PFC were prepared immediately after the second HTR tests. Higher-magnification images of anti-5-HT$_{2A}$ receptor immunostaining of arrow-pointed cells are presented with a gray scale. Yellow lines indicate the margins of somas outlined by NeuN-positive

Figure 5. *Continued*

signals, and the cyan arrowhead points to internalized anti-5-HT_{2A} receptor immunosignals. Scale bars, 20 μm. Images are representative of five mice.

(E) Quantification of internalized and membrane-associated 5-HT_{2A} receptor-positive areas relative to NeuN-positive area in mouse PFC. Thirty-five to forty NeuN-positive neuronal somas were analyzed for each sample (left chart: $p < 0.001$, right chart: $p = 0.011$, unpaired t test; n = 5 mice for each group).

Data are represented as means ± SEM. *$p < 0.05$, **$p < 0.01$, ***$p < 0.001$; ns, not significant. See also Figures S2 and S8.

exercise. Our findings suggest that the effects of walking and running on emotional regulation (Edwards et al., 2017) may involve serotonergic modulations in the cerebral cortex induced by mechanical impact on the head.

The amplitude of intracerebral pressure waves generated by PHM (frequency, 2 Hz) reproducing the peak acceleration magnitude at the heads induced by treadmill running was low (~1 mm Hg) when compared with that produced in synchronization with respiration (amplitude, ~2 mm Hg; frequency, ~0.5 Hz) (Figures 2B–2D). Intracerebral pressure waves with lower amplitude (~0.4 mm Hg) were also observed independent of respiration and PHM (Figures 2B–2D). Judging from the frequency of ~0.4 mm Hg pressure waves (~6.6 Hz), they are likely to derive from arterial pulsation or heartbeat. During the intracerebral pressure measurement, rats, either left sedentary or subjected to PHM, kept on breathing with their hearts beating. Therefore, neither ~2 mm Hg nor ~0.4 mm Hg intracerebral pressure waves could account for the PHM-specific interstitial fluid movement (Figures 2G, 2H, S5A, and S5B). Given the structural organization of interstitium that has been recently reported in many organs (Benias et al., 2018), the main element behind the physics of PHM-induced intracerebral interstitial fluid flow may not be the magnitude of pressure changes. Instead, other factors such as frequency and direction of accelerations may be critical for interstitial fluid flow generation in the PFC. In line with this notion, PHM effects on HTR and 5-HT_{2A} receptor internalization in the PFC neurons were dependent on the direction of PHM (Figures S6), supporting the importance of the direction of accelerations.

The roles of FSS in organismal homeostasis have been extensively documented for vascular endothelial cells with particular reference to its regularity and magnitude (Galie et al., 2015; Kadohama et al., 2007). In contrast, positive aspects of mechanical regulation of brain functions have been poorly documented, although nervous cells and systems can be mechanically modulated during physiological processes including normal development (Karkali and Martin-Blanco, 2017) and sleep induction (Kompotis et al., 2019). To date, mechanical stress on the head has mainly been implicated in damaging outcomes such as traumatic brain injury (Levy Nogueira et al., 2016). However, given the recent studies describing relatively "sparse" distribution of nervous cells in the brain (Murakami et al., 2018) as well as the importance of interstitium in organismal functions, it is reasonable to hypothesize that interstitial space plays significant regulatory roles in various brain-related capabilities and potentials.

The exercise (treadmill running)- or PHM-dependent desensitization of PFC neurons to 5-HT that we observed in this study may not simply represent the down-regulation of 5-HT_{2A} receptor signaling, but may contribute to the homeostasis in the brain. Exercise is known to increase 5-HT production and release in rodent brain (Chaouloff, 1989; Meeusen and De Meirleir, 1995). However, such effects of exercise are site and time dependent, as 5-HT concentration in rodent cerebral cortex stays unchanged (Blomstrand et al., 1989) or even decreases after exercise (Gomez-Merino et al., 2001). Therefore, 5-HT_{2A} receptor internalization observed after a week of daily treadmill running (Figures 1I, 1J, S3D, and S3E) is likely to be instigated ligand independently, rather than resulting from increased local 5-HT concentration in the PFC. In addition, extracellular 5-HT concentration in rat brain has been reported to be significantly decreased by isoflurane anesthesia (Mukaida et al., 2007), which was used during our PHM experiments. Ligand-dependent internalization of 5-HT_{2A} receptor (Schmid et al., 2008) thus appeared unlikely to be responsible for the PHM-induced suppression of HTR.

We demonstrate that PKCγ is involved in FSS-induced 5-HT_{2A} receptor internalization in neuronal cells *in vitro* and inhibition of PKC eliminates the effects of PHM on PFC neurons *in vivo* (Figure 4 and S7). PKCγ, a member of conventional PKC (cPKC) family, is exclusively expressed post-synaptically in neurons of the central nervous system and is involved in several neuronal functions, including long-term potentiation and long-term depression (Hashimoto et al., 1988; Saito and Shirai, 2002). However, the role of PKCγ in exercise effects on brain functions has not been distinctly documented to date, although it has been reported that long-term exposure to a running wheel remarkably increased PKCγ expression and activity in hippocampal and cortical tissues of adult

mice (Rao et al., 2015). Other cPKC family members are known to be involved in cellular responses to mechanical stresses (Traub and Berk, 1998), whereas mechanical regulation of PKCγ has not been demonstrated thus far. We speculate that such lack of studies on mechanical role of PKCγ may be partly due to the absence of notion that physiological functions of brain can be mechanically regulated.

Biocompatible hydrogel introduction in mouse PFCs eliminated the suppressive effect of PHM on HTR (Figure 5). Gelation of interstitial fluid may have three possible mechanisms damaging the surrounding tissue: (1) mechanical stress caused by high elastic modulus, (2) compression of surrounding tissue by swelling pressure, and (3) chemical stimulus by functional groups. To minimize the possibilities of these undesired consequences, the polymer concentration of pre-gel solutions was lowered to 25 g/L, which was confirmed to have negligible adverse effect on nerves in rabbit eyes (Hayashi et al., 2017). In our study, hydrogel introduction neither delayed HTR after 5-HTP administration (Figure S8D) nor altered 5-HT_{2A} receptor expression in the PFC (Figures S8E and S8F). Furthermore, neuronal survival or apoptosis was unaltered in hydrogel-introduced mouse PFCs (Figures S8G and S8H). Collectively, the loss of suppressive effect of PHM on HTR (Figures 5B and 5C) is likely to result from hydrogel-mediated alteration in interstitial fluid dynamics. Still, there may be unspecified effects of hydrogel introduction on the PFC neurons, particularly given that the hydrogel may alter the stiffness of extracellular matrix and the elasticity of the brain, which is known to affect the neurological physiology, pathology, and development (Li et al., 2017).

We expect that the effect of mechanical forces is not only limited to 5-HT_{2A} receptor signaling in the PFC but also relates to other cellular and molecular events involved in normal or healthy brain functions and conditions. Yet, the strict specificity of HTR for 5-HT_{2A} receptor signaling intensity in rodents' PFC neurons (Gonzalez-Maeso et al., 2007) enabled us to specifically dissect the effects of exercise (treadmill running) or PHM from complex brain functions. Our imaging-based analysis of the interstitial fluid dynamics combined with our simulative calculation indicates that intracerebral interstitial cells are subjected to FSS with an average magnitude of a few pascals, which coincides with the shear stress that protects vascular endothelial cells from inflammatory reactions (Hahn and Schwartz, 2009) or renders osteocytes mechanosensory cells in the context of mechanical loading-dependent bone homeostasis (Tatsumi et al., 2007; Weinbaum et al., 1994). Given the similarities between nervous and other types of cells with regard to intracellular signal activation by mechanical stretching (Lindqvist et al., 2010; Oldenhof et al., 2002; Sawada et al., 2001), mechano-responsive machinery may be commonly shared by a variety of different types of cells. We speculate that FSS with magnitude of a few pascals might be universally involved in organismal homeostasis. The significant contribution of cerebrospinal fluid flow to the brain homeostasis has been shown particularly in the system for waste clearance called the *glymphatic pathway'* (Iliff et al., 2012), whereas our study sheds light on another facet of the importance of extravascular fluid movement in the brain.

In summary, we have shown that mechanical perturbation on the head can modulate physiological brain functions of rodents. Further studies on the nervous system from mechanobiological perspectives will provide cues to unforeseen approaches to clinical problems related to brain malfunction and contribute to development of novel simple, safe, inexpensive, and broadly applicable therapeutic/preventative procedures for human brain diseases and disorders.

Limitations of the Study

There are several limitations of this study. We were unable to use mice in some of the animal experiments carried out in this project. Because of the issue on body size of mice, we needed to use rats to analyze physical matters and factors related to our study, including the measurement of accelerations at the heads. Although HTR is observed both in mice and rats (Bedard and Pycock, 1977; Goodwin and Green, 1985), we cannot thoroughly exclude the possibility that there are some differences in the mechanical regulations of 5-HT_{2A} receptor signaling in their PFC neurons.

We were also unable to test the response of primary neurons, which were prepared from mouse cerebral cortex or hippocampus, to FSS of reasonable magnitudes because of their easy detachment from the substrates by FSS. However, FSS is known to activate PKC (Kroll et al., 1993; Traub and Berk, 1998) and PKC-dependent GPCR internalization is observed in various types of cells (Chapell et al., 1998; Liles et al., 1986; Park et al., 2009). Furthermore, many of the cellular responses to mechanical forces lack strict cell specificity (Iskratsch et al., 2014). Taken together, we anticipate that 5-HT_{2A} receptor internalization represents a physiological response of neurons to FSS.

Although electrical stimulation was turned on only once or twice during the first 5 min of the 30-min treadmill running on the first day of the 1-week treadmill running period as mentioned previously, we cannot entirely preclude the possible effects of mental stress concomitant with forced treadmill running. In addition, considering possible unspecified influences of hydrogel on mouse PFC, elimination of the effects of PHM by hydrogel introduction (Figure 5) may not entirely confirm or solidify the role of intracerebral interstitial fluid flow in PHM-induced HTR suppression and 5-HT_{2A} receptor internalization. Further studies are required to address these issues.

METHODS

All methods can be found in the accompanying Transparent Methods supplemental file.

DATA AND CODE AVAILABILITY

All relevant data are available from the corresponding author upon reasonable request.

SUPPLEMENTAL INFORMATION

Supplemental Information can be found online at https://doi.org/10.1016/j.isci.2020.100874.

ACKNOWLEDGMENTS

We thank Dr. Y. Ikegaya and Ms. R. Kono (The University of Tokyo) for their technical support to primary neuron culture. This work was in part supported by Intramural Research Fund from the Japanese Ministry of Health, Labour and Welfare; Grants-in-Aid for Scientific Research from the Japan Society for the Promotion of Science (to T.O. and Y.S.); and MEXT-Supported Program for the Strategic Research Foundation at Private Universities, 2015-2019 from the Japanese Ministry of Education, Culture, Sports, Science and Technology (S1511017).

AUTHOR CONTRIBUTIONS

Y.R. proposed the initial idea related to HTR analysis in this project. Y.S. conceived and designed the study, supervised and led the project, and wrote the manuscript. Y.R. and T.M. conducted most of the experiments. D.Y. helped *in vitro* FSS experiments and carried out simulative calculation of *in vivo* fluid shear stress. N.S. conducted the experiments using primary neurons and μCT analysis. T.M., A.T., J.S., T.I., and S.M. contributed to the design and construction of the machine for PHM. J.T. and M.M. contributed to the acquisition and the analysis of MRI data, respectively. T.S. and Y.Y. developed and provided the PEG hydrogel system. M.N., N.F., K.S., S.W., T.T., M.W., H.H., T.O., and M.S. provided technical, advisory and financial support.

DECLARATION OF INTERESTS

Y.R., T.M., A.T., T.I., J.S., S.M., T.O., and Y.S. joined the application for a patent related to this work, which has been granted in Japan (JP6592834) and filed internationally (US16/616,935; EP18806753.2; CN201880033284.0; IN201927048891), as inventors.

Received: May 6, 2019
Revised: January 15, 2020
Accepted: January 27, 2020
Published: February 21, 2020

REFERENCES

Aghajanian, G.K., and Marek, G.J. (1999). Serotonin and hallucinogens. Neuropsychopharmacology *21*, 16s–23s.

Bedard, P., and Pycock, C.J. (1977). "Wet-dog" shake behaviour in the rat: a possible quantitative model of central 5-hydroxytryptamine activity. Neuropharmacology *16*, 663–670.

Benias, P.C., Wells, R.G., Sackey-Aboagye, B., Klavan, H., Reidy, J., Buonocore, D., Miranda, M., Kornacki, S., Wayne, M., Carr-Locke, D.L., et al. (2018). Structure and distribution of an unrecognized interstitium in human tissues. Sci. Rep. *8*, 4947.

Berger, M., Gray, J.A., and Roth, B.L. (2009). The expanded biology of serotonin. Annu. Rev. Med. *60*, 355–366.

Berk, B.C., Corson, M.A., Peterson, T.E., and Tseng, H. (1995). Protein kinases as mediators of fluid shear stress stimulated signal transduction in endothelial cells: a hypothesis for calcium-dependent and calcium-independent events activated by flow. J. Biomech. *28*, 1439–1450.

Bhattacharyya, S., Puri, S., Miledi, R., and Panicker, M.M. (2002). Internalization and recycling of 5-HT_{2A} receptors activated by serotonin and protein kinase C-mediated mechanisms. Proc. Natl. Acad. Sci. U S A. *99*, 14470–14475.

Blomstrand, E., Perrett, D., Parry-Billings, M., and Newsholme, E.A. (1989). Effect of sustained exercise on plasma amino acid concentrations and on 5-hydroxytryptamine metabolism in six different brain regions in the rat. Acta Physiol. Scand. *136*, 473–481.

Bowers, B.J., Miyamoto-Ditmon, J., and Wehner, J.M. (2006). Regulation of 5-$HT_{2A/C}$ receptors and DOI-induced behaviors by protein kinase Cγ. Pharmacol. Biochem. Behav. *85*, 441–447.

Canal, C.E., and Morgan, D. (2012). Head-twitch response in rodents induced by the hallucinogen 2,5-dimethoxy-4-iodoamphetamine: a comprehensive history, a re-evaluation of mechanisms, and its utility as a model. Drug Test. Anal. *4*, 556–576.

Canli, T., and Lesch, K.P. (2007). Long story short: the serotonin transporter in emotion regulation and social cognition. Nat. Neurosci. *10*, 1103–1109.

Chaar, L.J., Alves, T.P., Batista Junior, A.M., and Michelini, L.C. (2015). Early training-induced reduction of angiotensinogen in autonomic areas-the main effect of exercise on brain renin-angiotensin system in hypertensive rats. PLoS One *10*, e0137395.

Chaouloff, F. (1989). Physical exercise and brain monoamines: a review. Acta Physiol. Scand. *137*, 1–13.

Chapell, R., Bueno, O.F., Alvarez-Hernandez, X., Robinson, L.C., and Leidenheimer, N.J. (1998). Activation of protein kinase C induces γ-aminobutyric acid type A receptor internalization in xenopus oocytes. J. Biol. Chem. *273*, 32595–32601.

Cornea-Hebert, V., Riad, M., Wu, C., Singh, S.K., and Descarries, L. (1999). Cellular and subcellular distribution of the serotonin 5-HT_{2A} receptor in the central nervous system of adult rat. J. Comp. Neurol. *409*, 187–209.

Diaz, S.L., and Maroteaux, L. (2011). Implication of 5-HT_{2B} receptors in the serotonin syndrome. Neuropharmacology *61*, 495–502.

Edwards, M.K., Rhodes, R.E., and Loprinzi, P.D. (2017). A randomized control intervention investigating the effects of acute exercise on emotional regulation. Am. J. Health Behav. *41*, 534–543.

Egan, C.T., Herrick-Davis, K., Miller, K., Glennon, R.A., and Teitler, M. (1998). Agonist activity of LSD and lisuride at cloned 5-HT_{2A} and 5-HT_{2C} receptors. Psychopharmacology (Berl) *136*, 409–414.

Fujiyabu, T., Toni, F., Li, X., Chung, U.I., and Sakai, T. (2018). Three cooperative diffusion coefficients describing dynamics of polymer gels. Chem. Commun. (Camb) *54*, 6784–6787.

Galie, P.A., van Oosten, A., Chen, C.S., and Janmey, P.A. (2015). Application of multiple levels of fluid shear stress to endothelial cells plated on polyacrylamide gels. Lab Chip *15*, 1205–1212.

Gomez-Merino, D., Bequet, F., Berthelot, M., Chennaoui, M., and Guezennec, C.Y. (2001). Site-dependent effects of an acute intensive exercise on extracellular 5-HT and 5-HIAA levels in rat brain. Neurosci. Lett. *301*, 143–146.

Gonzalez-Maeso, J., Weisstaub, N.V., Zhou, M., Chan, P., Ivic, L., Ang, R., Lira, A., Bradley-Moore, M., Ge, Y., Zhou, Q., et al. (2007). Hallucinogens recruit specific cortical 5-HT_{2A} receptor-mediated signaling pathways to affect behavior. Neuron *53*, 439–452.

Goodwin, G.M., and Green, A.R. (1985). A behavioural and biochemical study in mice and rats of putative selective agonists and antagonists for 5-HT_1 and 5-HT_2 receptors. Br. J. Pharmacol. *84*, 743–753.

Goshima, Y., Ohsako, S., and Yamauchi, T. (1993). Overexpression of Ca^{2+}/calmodulin-dependent protein kinase II in Neuro2A and NG108-15 neuroblastoma cell lines promotes neurite outgrowth and growth cone motility. J. Neurosci. *13*, 559–567.

Guiard, B.P., and Di Giovanni, G. (2015). Central serotonin-2A (5-HT_{2A}) receptor dysfunction in depression and epilepsy: the missing link? Front. Pharmacol. *6*, 46.

Hahn, C., and Schwartz, M.A. (2009). Mechanotransduction in vascular physiology and atherogenesis. Nat. Rev. Mol. Cell. Biol. *10*, 53–62.

Halberstadt, A.L., and Geyer, M.A. (2013). Characterization of the head-twitch response induced by hallucinogens in mice: detection of the behavior based on the dynamics of head movement. Psychopharmacology (Berl) *227*, 727–739.

Hartwig, J.H., Thelen, M., Rosen, A., Janmey, P.A., Nairn, A.C., and Aderem, A. (1992). MARCKS is an actin filament crosslinking protein regulated by protein kinase C and calcium-calmodulin. Nature *356*, 618–622.

Hashimoto, T., Ase, K., Sawamura, S., Kikkawa, U., Saito, N., Tanaka, C., and Nishizuka, Y. (1988). Postnatal development of a brain-specific subspecies of protein kinase C in rat. J. Neurosci. *8*, 1678–1683.

Haskell, W.L., Lee, I.M., Pate, R.R., Powell, K.E., Blair, S.N., Franklin, B.A., Macera, C.A., Heath, G.W., Thompson, P.D., and Bauman, A. (2007). Physical activity and public health: updated recommendation for adults from the American College of Sports Medicine and the American Heart Association. Med. Sci. Sports Exerc. *39*, 1423–1434.

Hayashi, K., Okamoto, F., Hoshi, S., Katashima, T., Zujur, D.C., Li, X., Shibayama, M., Gilbert, E.P., Chung, U.-i., and Ohba, S. (2017). Fast-forming hydrogel with ultralow polymeric content as an artificial vitreous body. Nat. Biomed. Eng. *1*, 0044.

Hyman, A.J., Tumova, S., and Beech, D.J. (2017). Piezo1 channels in vascular development and the sensing of shear stress. Curr. Top. Membr. *79*, 37–57.

Iliff, J.J., Wang, M., Liao, Y., Plogg, B.A., Peng, W., Gundersen, G.A., Benveniste, H., Vates, G.E., Deane, R., Goldman, S.A., et al. (2012). A paravascular pathway facilitates CSF flow through the brain parenchyma and the clearance of interstitial solutes, including amyloid beta. Sci. Transl. Med. *4*, 147ra111.

Iskratsch, T., Wolfenson, H., and Sheetz, M.P. (2014). Appreciating force and shape-the rise of mechanotransduction in cell biology. Nat. Rev. Mol. Cell Biol. *15*, 825–833.

Kadohama, T., Nishimura, K., Hoshino, Y., Sasajima, T., and Sumpio, B.E. (2007). Effects of different types of fluid shear stress on endothelial cell proliferation and survival. J. Cell. Physiol *212*, 244–251.

Karkali, K., and Martin-Blanco, E. (2017). Mechanosensing in the Drosophila nervous system. Semin. Cell Dev. Biol. *71*, 22–29.

Kim, S.E., Ko, I.G., Kim, B.K., Shin, M.S., Cho, S., Kim, C.J., Kim, S.H., Baek, S.S., Lee, E.K., and Jee, Y.S. (2010). Treadmill exercise prevents aging-induced failure of memory through an increase in neurogenesis and suppression of apoptosis in rat hippocampus. Exp. Gerontol. *45*, 357–365.

Kirk-Sanchez, N.J., and McGough, E.L. (2014). Physical exercise and cognitive performance in the elderly: current perspectives. Clin. Interv. Aging *9*, 51–62.

Klein-Nulend, J., Bakker, A.D., Bacabac, R.G., Vatsa, A., and Weinbaum, S. (2013). Mechanosensation and transduction in osteocytes. Bone *54*, 182–190.

Kompotis, K., Hubbard, J., Emmenegger, Y., Perrault, A., Muhlethaler, M., Schwartz, S., Bayer, L., and Franken, P. (2019). Rocking promotes sleep in mice through rhythmic stimulation of the vestibular system. Curr. Biol. *29*, 392–401.e4.

Kroll, M.H., Hellums, J.D., Guo, Z., Durante, W., Razdan, K., Hrbolich, J.K., and Schafer, A.I. (1993). Protein kinase C is activated in platelets subjected to pathological shear stress. J. Biol. Chem. *268*, 3520–3524.

Levy Nogueira, M., Lafitte, O., Steyaert, J.M., Bakardjian, H., Dubois, B., Hampel, H., and Schwartz, L. (2016). Mechanical stress related to brain atrophy in Alzheimer's disease. Alzheimers Dement. *12*, 11–20.

Li, H., Liang, A., Guan, F., Fan, R., Chi, L., and Yang, B. (2013). Regular treadmill running improves spatial learning and memory performance in young mice through increased hippocampal neurogenesis and decreased stress. Brain Res. *1531*, 1–8.

Li, S.C., Vu, L.T., Luo, J.J., Zhong, J.F., Li, Z., Dethlefs, B.A., Loudon, W.G., and Kabeer, M.H. (2017). Tissue elasticity bridges cancer stem cells to the tumor microenvironment through microRNAs: Implications for a "watch-and-wait" approach to cancer. Curr. Stem Cell Res. Ther. *12*, 455–470.

Liles, W.C., Hunter, D.D., Meier, K.E., and Nathanson, N.M. (1986). Activation of protein kinase C induces rapid internalization and subsequent degradation of muscarinic acetylcholine receptors in neuroblastoma cells. J. Biol. Chem. *261*, 5307–5313.

Lindqvist, N., Liu, Q., Zajadacz, J., Franze, K., and Reichenbach, A. (2010). Retinal glial (Muller) cells: sensing and responding to tissue stretch. Invest. Ophthalmol. Vis. Sci. *51*, 1683–1690.

Maneshi, M.M., Maki, B., Gnanasambandam, R., Belin, S., Popescu, G.K., Sachs, F., and Hua, S.Z. (2017). Mechanical stress activates NMDA

receptors in the absence of agonists. Sci. Rep. *7*, 39610.

Marek, G.J., and Aghajanian, G.K. (1996). LSD and the phenethylamine hallucinogen DOI are potent partial agonists at 5-HT_{2A} receptors on interneurons in rat piriform cortex. J. Pharmacol. Exp. Ther. *278*, 1373–1382.

Meeusen, R., and De Meirleir, K. (1995). Exercise and brain neurotransmission. Sports Med. *20*, 160–188.

Menard, C., Bastianetto, S., and Quirion, R. (2013). Neuroprotective effects of resveratrol and epigallocatechin gallate polyphenols are mediated by the activation of protein kinase Cγ. Front. Cell Neurosci. *7*, 281.

Mukaida, K., Shichino, T., Koyanagi, S., Himukashi, S., and Fukuda, K. (2007). Activity of the serotonergic system during isoflurane anesthesia. Anesth. Analg. *104*, 836–839.

Murakami, T.C., Mano, T., Saikawa, S., Horiguchi, S.A., Shigeta, D., Baba, K., Sekiya, H., Shimizu, Y., Tanaka, K.F., Kiyonari, H., et al. (2018). A three-dimensional single-cell-resolution whole-brain atlas using CUBIC-X expansion microscopy and tissue clearing. Nat. Neurosci. *21*, 625–637.

Nichols, D.E. (2004). Hallucinogens. Pharmacol. Ther. *101*, 131–181.

Oldenhof, A.D., Shynlova, O.P., Liu, M., Langille, B.L., and Lye, S.J. (2002). Mitogen-activated protein kinases mediate stretch-induced c-fos mRNA expression in myometrial smooth muscle cells. Am. J. Physiol. Cell Physiol. *283*, C1530–C1539.

Oury, F., Khrimian, L., Denny, C.A., Gardin, A., Chamouni, A., Goeden, N., Huang, Y.Y., Lee, H., Srinivas, P., Gao, X.B., et al. (2013). Maternal and offspring pools of osteocalcin influence brain development and functions. Cell *155*, 228–241.

Park, J.S., Voitenko, N., Petralia, R.S., Guan, X., Xu, J.T., Steinberg, J.P., Takamiya, K., Sotnik, A., Kopach, O., Huganir, R.L., et al. (2009). Persistent inflammation induces GluR2 internalization via NMDA receptor-triggered PKC activation in dorsal horn neurons. J. Neurosci. *29*, 3206–3219.

Preller, K.H., Schilbach, L., Pokorny, T., Flemming, J., Seifritz, E., and Vollenweider, F.X. (2018). Role of the 5-HT_{2A} receptor in self- and other-initiated social interaction in lysergic acid diethylamide-induced states: a pharmacological fMRI study. J. Neurosci. *38*, 3603–3611.

Puig, M.V., and Gulledge, A.T. (2011). Serotonin and prefrontal cortex function: neurons, networks, and circuits. Mol. Neurobiol. *44*, 449–464.

Rao, S.K., Ross, J.M., Harrison, F.E., Bernardo, A., Reiserer, R.S., Reiserer, R.S., Mobley, J.A., and McDonald, M.P. (2015). Differential proteomic and behavioral effects of long-term voluntary exercise in wild-type and APP-overexpressing transgenics. Neurobiol. Dis. *78*, 45–55.

Roth, B.L., Hanizavareh, S.M., and Blum, A.E. (2004). Serotonin receptors represent highly favorable molecular targets for cognitive enhancement in schizophrenia and other disorders. Psychopharmacology (Berl) *174*, 17–24.

Ryu, Y., Ogata, T., Nagao, M., Sawada, Y., Nishimura, R., and Fujita, N. (2018). Effects of treadmill training combined with serotonergic interventions on spasticity after contusive spinal cord injury. J. Neurotrauma *35*, 1358–1366.

Saito, N., and Shirai, Y. (2002). Protein kinase Cγ (PKCγ): function of neuron specific isotype. J. Biochem. *132*, 683–687.

Sawada, Y., Nakamura, K., Doi, K., Takeda, K., Tobiume, K., Saitoh, M., Morita, K., Komuro, I., De Vos, K., Sheetz, M., et al. (2001). Rap1 is involved in cell stretching modulation of p38 but not ERK or JNK MAP kinase. J. Cell Sci. *114*, 1221–1227.

Schmid, C.L., Raehal, K.M., and Bohn, L.M. (2008). Agonist-directed signaling of the serotonin 2A receptor depends on β-arrestin-2 interactions in vivo. Proc. Natl. Acad. Sci. U S A. *105*, 1079–1084.

Siddiqui, S.V., Chatterjee, U., Kumar, D., Siddiqui, A., and Goyal, N. (2008). Neuropsychology of prefrontal cortex. Indian J. Psychiatry *50*, 202.

Tatsumi, S., Ishii, K., Amizuka, N., Li, M., Kobayashi, T., Kohno, K., Ito, M., Takeshita, S., and Ikeda, K. (2007). Targeted ablation of osteocytes induces osteoporosis with defective mechanotransduction. Cell Metab. *5*, 464–475.

Traub, O., and Berk, B.C. (1998). Laminar shear stress: mechanisms by which endothelial cells transduce an atheroprotective force. Arterioscler. Thromb. Vasc. Biol. *18*, 677–685.

Tworkoski, E., Glucksberg, M.R., and Johnson, M. (2018). The effect of the rate of hydrostatic pressure depressurization on cells in culture. PLoS One *13*, e0189890.

van Praag, H., Fleshner, M., and Schwartz, M.W. (2014). Exercise, energy intake, glucose homeostasis, and the brain. J. Neurosci. *34*, 15139–15149.

Wang, P.W., Lin, H.C., Su, C.Y., Chen, M.D., Lin, K.C., Ko, C.H., and Yen, C.F. (2018). Effect of aerobic exercise on improving symptoms of individuals with schizophrenia: a single blinded randomized control study. Front. Psychiatry *9*, 167.

Weinbaum, S., Cowin, S.C., and Zeng, Y. (1994). A model for the excitation of osteocytes by mechanical loading-induced bone fluid shear stresses. J. Biomech. *27*, 339–360.

Weisstaub, N.V., Zhou, M., Lira, A., Lambe, E., Gonzalez-Maeso, J., Hornung, J.P., Sibille, E., Underwood, M., Itohara, S., Dauer, W.T., et al. (2006). Cortical 5-HT_{2A} receptor signaling modulates anxiety-like behaviors in mice. Science *313*, 536–540.

Wrann, C.D. (2015). FNDC5/irisin - their role in the nervous system and as a mediator for beneficial effects of exercise on the brain. Brain Plast. *1*, 55–61.

Yoshino, D., Sakamoto, N., Takahashi, K., Inoue, E., and Sato, M. (2013). Development of novel flow chamber to study endothelial cell morphology: effects of shear flow with uniform spatial gradient on distribution of focal adhesion. J. Biomech. Sci. Eng. *8*, 233–243.

Yun, J., Nagai, T., Furukawa-Hibi, Y., Kuroda, K., Kaibuchi, K., Greenberg, M.E., and Yamada, K. (2013). Neuronal Per Arnt Sim (PAS) domain protein 4 (NPAS4) regulates neurite outgrowth and phosphorylation of synapsin I. J. Biol. Chem. *288*, 2655–2664.

Zhang, G., Asgeirsdottir, H.N., Cohen, S.J., Munchow, A.H., Barrera, M.P., and Stackman, R.W., Jr. (2013). Stimulation of serotonin 2A receptors facilitates consolidation and extinction of fear memory in C57BL/6J mice. Neuropharmacology *64*, 403–413.

Zou, Y., Akazawa, H., Qin, Y., Sano, M., Takano, H., Minamino, T., Makita, N., Iwanaga, K., Zhu, W., Kudoh, S., et al. (2004). Mechanical stress activates angiotensin II type 1 receptor without the involvement of angiotensin II. Nat. Cell Biol. *6*, 499–506.

iScience, Volume *23*

Supplemental Information

Mechanical Regulation Underlies Effects of Exercise on Serotonin-Induced Signaling in the Prefrontal Cortex Neurons

Youngjae Ryu, Takahiro Maekawa, Daisuke Yoshino, Naoyoshi Sakitani, Atsushi Takashima, Takenobu Inoue, Jun Suzurikawa, Jun Toyohara, Tetsuro Tago, Michiru Makuuchi, Naoki Fujita, Keisuke Sawada, Shuhei Murase, Masashi Watanave, Hirokazu Hirai, Takamasa Sakai, Yuki Yoshikawa, Toru Ogata, Masahiro Shinohara, Motoshi Nagao, and Yasuhiro Sawada

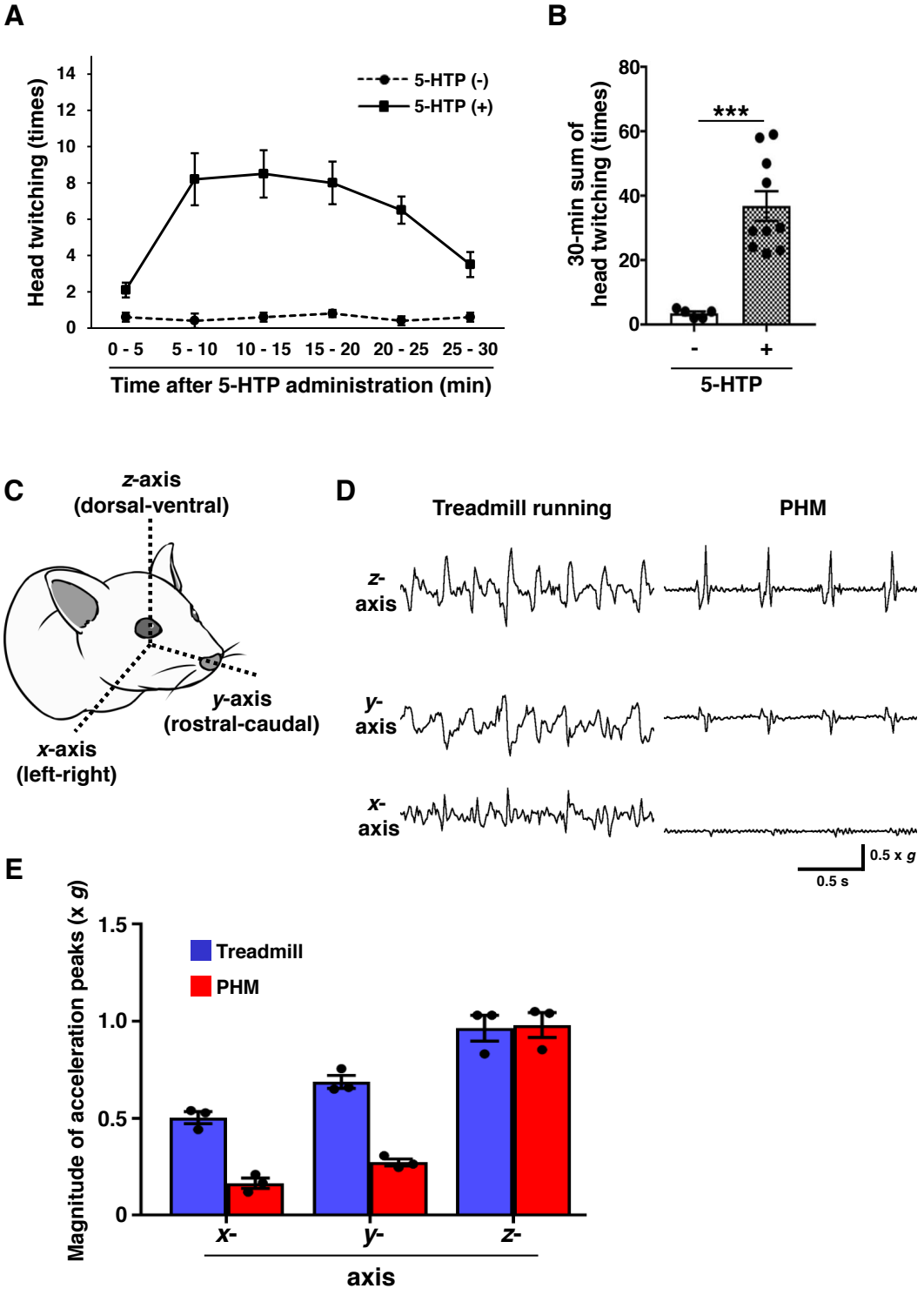

Figure S1. Counting Head Twitching after 5-HTP Administration and Measurement of Accelerations Generated at Rats' Heads during Treadmill Running and PHM, Related to Figure 1

(A and B) Quantification of 5-HTP-induced HTR. Line chart of head twitching count in 5-min blocks for 30 min (A) and histogram of total head twitching count (B) after administration of 5-HTP (5-HTP; n = 10) or saline (Control; n = 5). $^{***}p < 0.001$ (unpaired t test).

(C) Definition of *x*-(left-right), *y*-(rostral-caudal), and *z*-(dorsal-ventral) axes used in this study.

(D) Accelerations generated at the rats' heads during treadmill running (velocity: 20 m/min) and PHM (frequency: 2 Hz). The head drop by the PHM system was adjusted to 5 mm to produce 1.0 x *g* vertical acceleration peaks. Right-angled scale bar, 0.5 x *g* / 0.5 s. Images are representative of three independent experiments with similar results.

(E) Peak magnitudes of accelerations for *x*-, *y*-, and *z*-axes during treadmill running and PHM (n = 3 rats for each group).

Data are represented as means ± SEM.

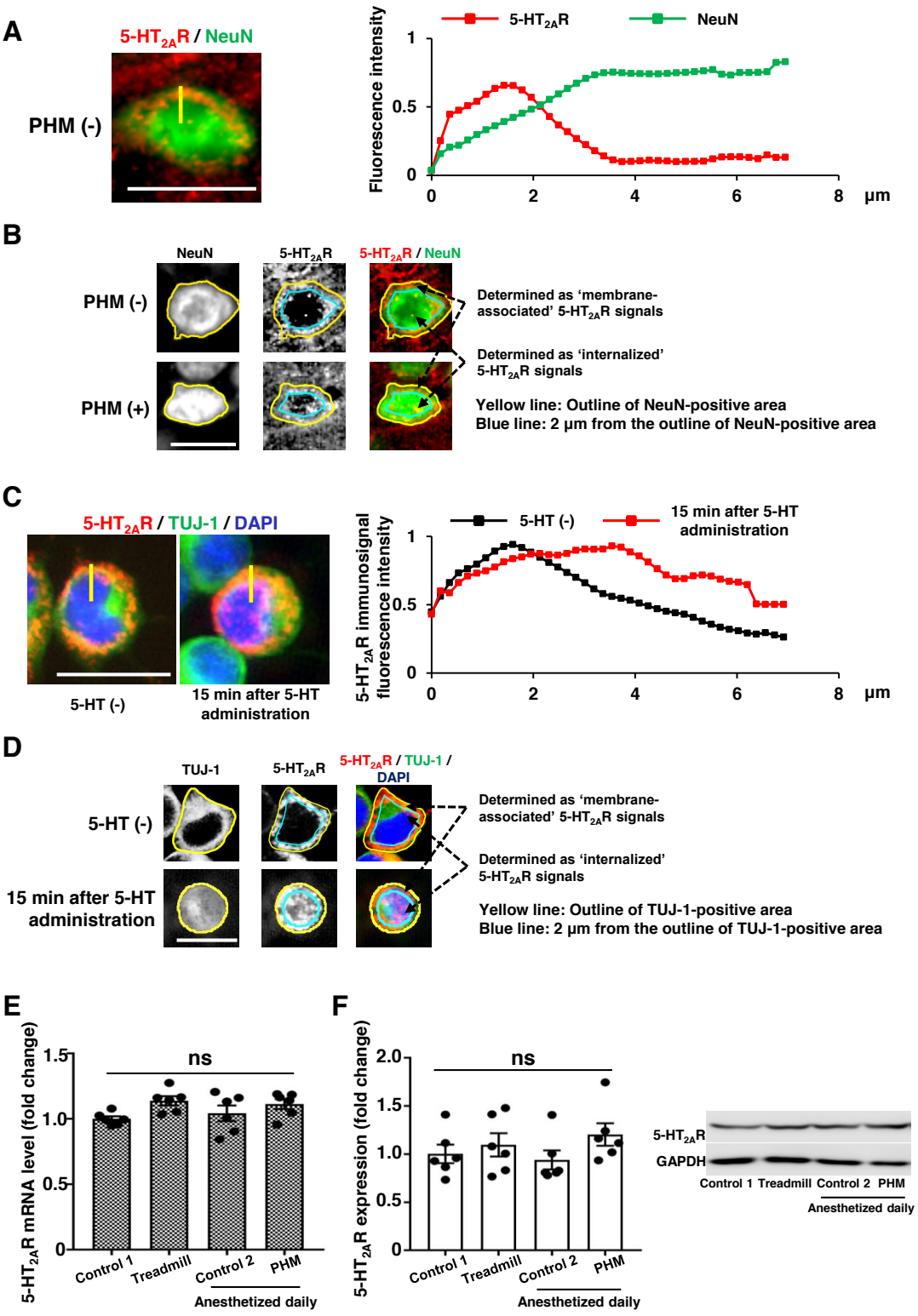

Figure S2. Representation of 5-HT$_{2A}$ Receptor Internalization in Mouse PFC Neurons and Neuro2A Cells, Related to Figures 1, 3, 4, 5, S3, S4, S6, and S7

(A) Anti-5-HT_{2A} receptor immunosignals along the soma margins of mouse PFC neurons were predominantly distributed within 2 μm from their outlines. Intensities of anti-5-HT_{2A} receptor (5-HT_{2A}R; red) and anti-NeuN (green) immunosignals were quantified along the line perpendicular to the soma outlines defined by anti-NeuN immunosignals. Scale bar, 20 μm (left). Relative signal intensities were scaled with the highest intensity in the individual cells set at 1. The graphed lines represent the mean values from 10 PFC neurons with apparent marginal distribution of anti-5-HT_{2A} receptor immunosignals (right).

(B) Schematic representation of the definition as to 'membrane-associated' and 'internalized' anti-5-HT_{2A} receptor immunosignals used for the quantification in Figures 1J, 5E, S3E, S3J, S4E, S4J, S6E, S6J, and S7D. Yellow lines indicate the outlines of somas defined by anti-NeuN immunosignals. Blue lines represent 2 μm inside the soma outlines. Scale bar, 20 μm.

(C) Quantification of the distribution of anti-5-HT_{2A} receptor immunosignals in Neuro2A cells with and without 5-HT treatment. The intensity of anti-5-HT_{2A} receptor (5-HT_{2A}R; red) immunosignals were quantified along the line perpendicular to the soma outlines of Neuro2A, either treated or left untreated with 5-HT (10 μM, 15 min). Intensities of anti-5-HT_{2A} receptor immunosignals were quantified along the line perpendicular to the soma outlines defined by anti-TUJ-1 (green) immunosignals (left), and scaled as in (A). Scale bar, 20 μm. The graphed lines individually represent the mean values from 20 Neuro2A cells with and without 5-HT treatment (right).

(D) Schematic representation of the definition as to 'membrane-associated' and 'internalized' anti-5-HT_{2A} receptor (5-HT_{2A}R; red) immunosignals used for the quantification in Figures 3C and 4D. Yellow lines indicate the outlines of neuronal

somas defined by anti-TUJ-1 (green) immunosignals. Blue lines represent 2 μm inside from the soma outlines. Scale bar, 20 μm.

(E and F) Neither treadmill running nor PHM significantly alters the expression level of 5-HT_{2A} receptor in mouse PFC. mRNA (E) and protein (F) expressions of 5-HT_{2A} receptor in mouse PFC were quantified with the mean values of control 1 set as 1 ($p = 0.095$ and $p = 0.36$ for ns, one-way ANOVA with post hoc Bonferroni test; $n = 6$ mice for each group). Controls 1 and 2 were defined as in Figure 1. Data are represented as means ± SEM. ns, not significant.

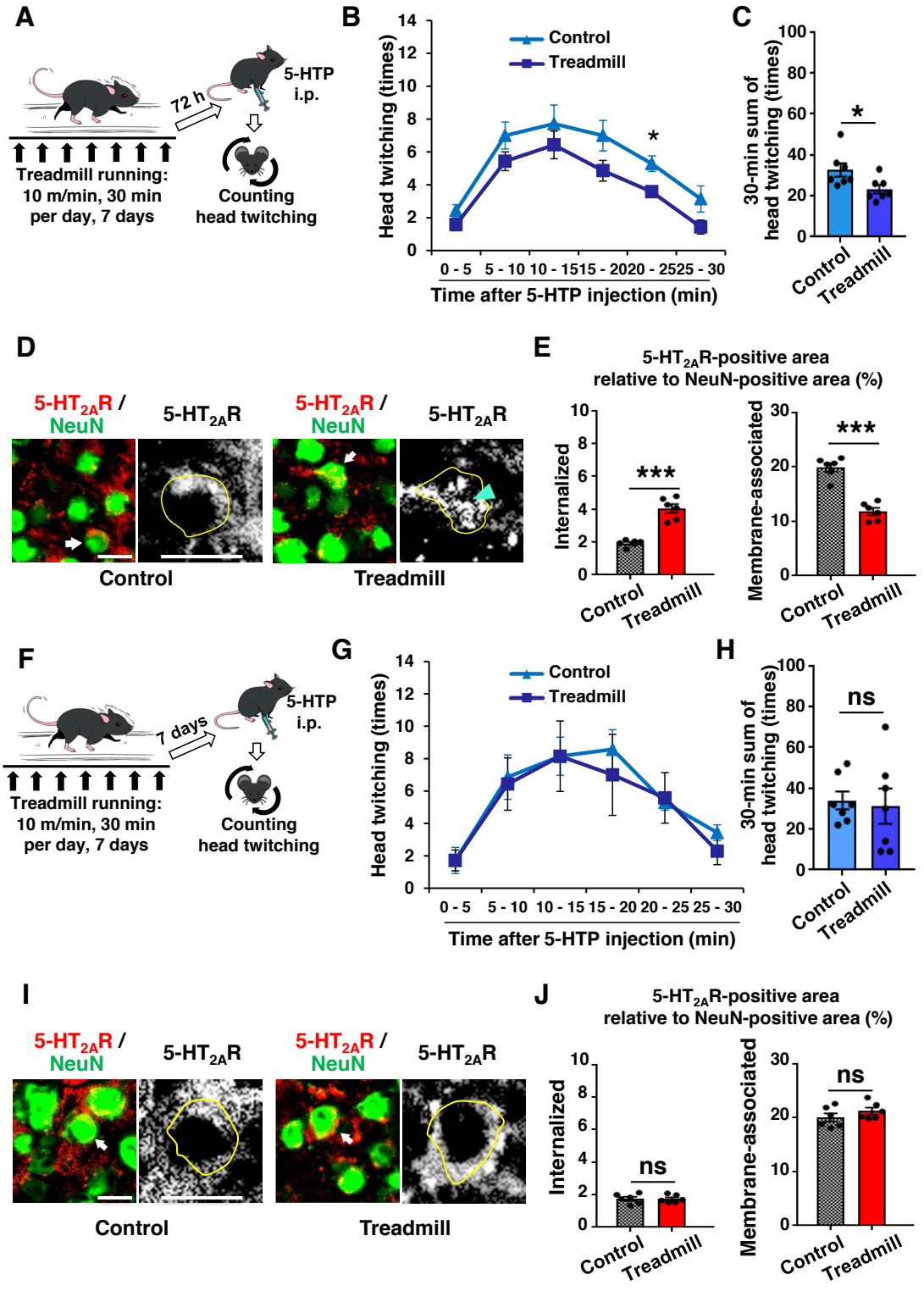

Figure S3. Longer-Term Effects of Treadmill Running on HTR and 5-HT$_{2A}$ Receptor Internalization in the PFC Neurons of Mice, Related to Figure 1

(A-E) The effects of 1-week daily treadmill running remain 72 h after its last bout. (A) Schematic representation of experimental protocol for analysis of 72-h effects of treadmill running on HTR. 5-HTP administration for HTR test was conducted 72 h after the last bout of 1-week daily treadmill running. (B and C) Count of head twitching in 5-min blocks (B) and for 30 min (C) post-5-HTP administration (C, $p = 0.033$, unpaired t test; n = 7 mice for each group). (D) Micrographic images of anti-5-HT_{2A} receptor (5-HT_{2A}R; red) and anti-NeuN (green) immunostaining of mouse PFC are presented as in Figure 1I. Scale bars, 20 μm. (E) Quantification of internalized and membrane-associated 5-HT_{2A} receptor-positive area relative to NeuN-positive area in mouse PFC is presented as in Figure 1J (internalized: $p < 0.001$, membrane-associated: $p < 0.001$, unpaired t test; n = 6 mice for each group).

(F-J) The effects of 1-week daily treadmill running do not remain 7 days after its last bout. (F) Schematic representation of experimental protocol for analysis of 7-day effects of treadmill running on HTR. 5-HTP administration for HTR test was conducted 7 days after the last bout of 1-week daily treadmill running. (G-J) HTR and 5-HT_{2A} receptor internalization in PFC neurons of mice were analyzed as in (B-E) (H, $p = 0.77$, unpaired t test; n = 7 mice for each group) (J, internalized: $p = 0.98$, membrane-associated: $p = 0.27$, unpaired t test; n = 6 mice for each group). Scale bars, 20 μm.

Controls in (B-E and G-J) represent mice that were placed on the belt of treadmill machine without turning on the treadmilling (30 min per day, 7 days). Data for the samples in (D, E, I and J) were obtained from mice infused with 4% PFA/PBS immediately after HTR test shown in (B, C, G and H). Data are represented as means ± SEM. $^{*}p < 0.05$; $^{***}p < 0.001$; ns, not significant. See also Figure S2.

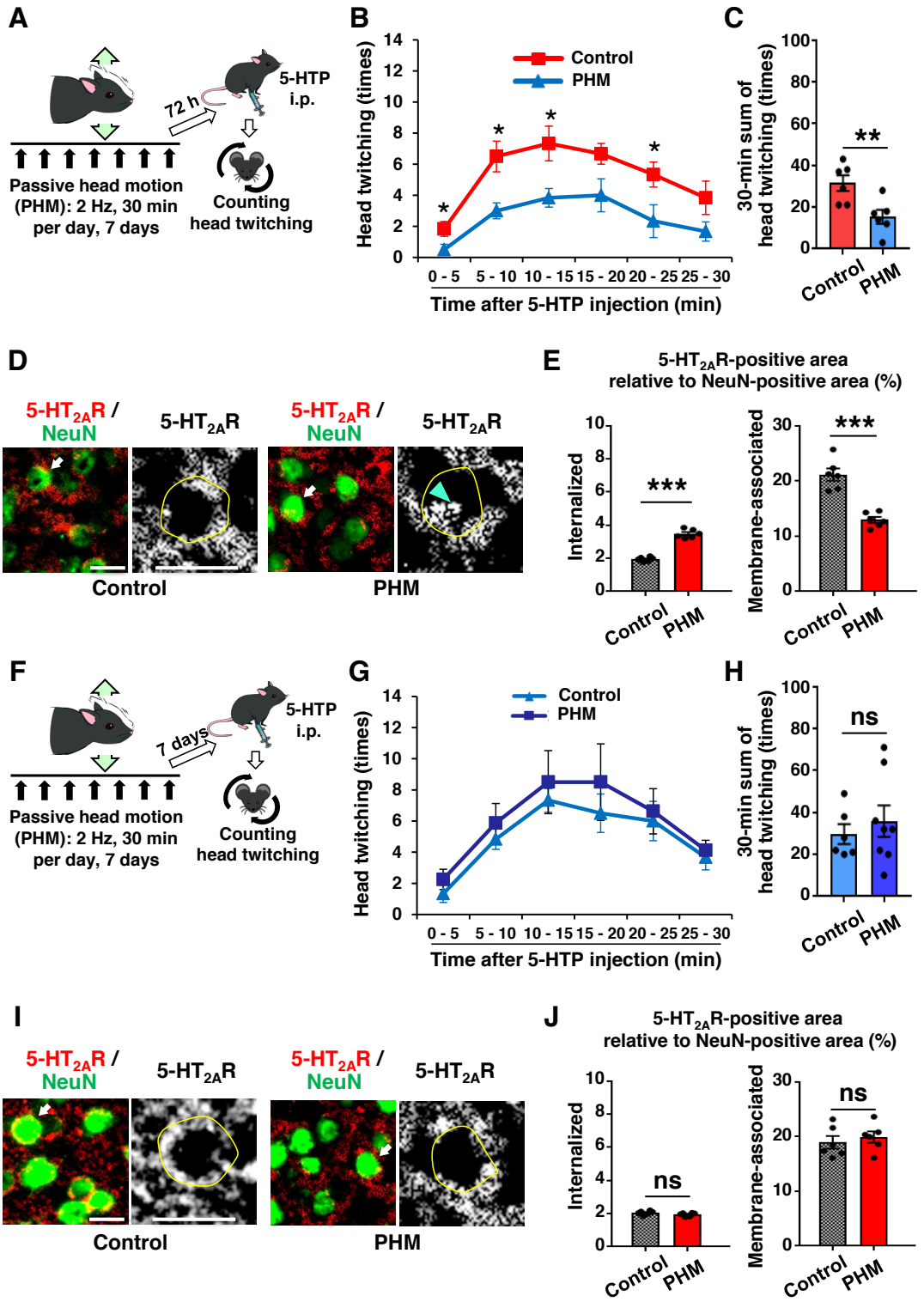

Figure S4. Longer-Term Effects of PHM on HTR and 5-HT$_{2A}$ Receptor Internalization in the PFC Neurons of Mice, Related to Figure 1

(A-E) The effects of 1-week daily PHM remain 72 h after its last bout. (A) Schematic representation of experimental protocol for analysis of 72-h effects of PHM on HTR. 5-HTP administration for HTR test was conducted 72 h after the last bout of 1-week daily PHM. (B-E) HTR and 5-HT_{2A} receptor internalization in PFC neurons of mice were analyzed as in Figures S3B-S3E (C, $p = 0.0095$, unpaired t test; n = 6 mice for each group) (E, internalized: $p < 0.001$, membrane-associated: $p < 0.001$, unpaired t test; n = 6 mice for each group). Scale bars, 20 μm.

(F-J) The effects of 1-week daily PHM do not remain 7 days after its last bout. (F) Schematic representation of experimental protocol for analysis of 7-day effects of treadmill running on HTR. 5-HTP administration for HTR test was conducted 7 days after the last bout of 1-week daily treadmill running. (G-J) HTR and 5-HT_{2A} receptor internalization in PFC neurons of mice were analyzed as in Figures S3B-S3E (H, $p = 0.53$, unpaired t test; n = 6 mice for control group, n = 8 mice for PHM group) (J, internalized: $p = 0.16$, membrane-associated: $p = 0.54$, unpaired t test; n = 6 mice for each group). Scale bars, 20 μm.

Controls in (B-E and G-J) represent mice that were anesthetized, and placed in a prone position with their heads on the platform that was left unoscillated (30 min per day, 7 days). Data for the samples in (D, E, I and J) were obtained from mice infused with 4% PFA/PBS immediately after HTR test shown in (B, C, G and H). Data are represented as means ± SEM. $^{*}p < 0.05$; $^{**}p < 0.01$; $^{***}p < 0.001$; ns, not significant. See also Figure S2.

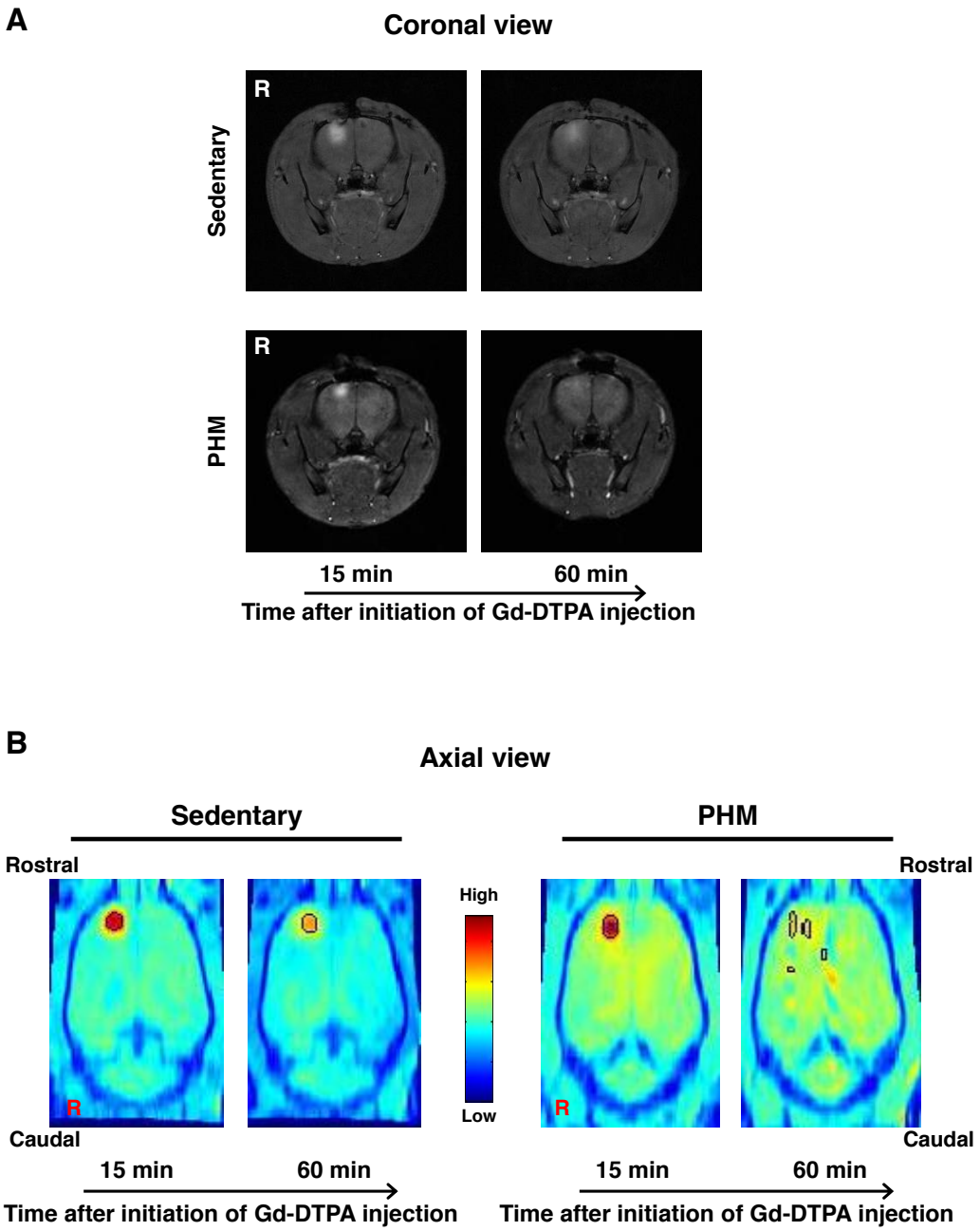

Figure S5. MRI Analysis of Spreading of Gd-DTPA Injected in Rats' PFC, Related to Figure 2

(A) Representative coronal view slices of MRI scanned before and after interventions (PHM or sedentary). 'R' indicates the right side. Each image is representative of five rats.

(B) Pseudo-color presentation of MR signal intensity. Gd-DTPA clusters were defined as voxels of top 0.05% intensity marked with black lines. The original MRI data for the slices shown in (A) and for the intensity shown in (B) are identical (from the same rats) in both sedentary and PHM-applied rats.

A

Property	Value
Pressure (ΔP; mm Hg)	0.93
Viscosity (μ; mPa·s)	1 - 20 #
Spread distance along *x*-axis (Δx; μm)	0.4074
Spread distance along *y*-axis (Δy; μm)	0.6222
Spread distance along *z*-axis (Δz; μm)	0.4370
Velocity of interstitial fluid flow along *x*-axis ($u_{\infty,x}$; μm/s)	0.8148
Velocity of interstitial fluid flow along *y*-axis ($u_{\infty,y}$; μm/s)	1.2592
Velocity of interstitial fluid flow along *z*-axis ($u_{\infty,z}$; μm/s)	0.8741

B

Fluid shear stress (τ_x) along *x*-axis at the cell surface:

$$\tau_x = \frac{\mu u_{\infty,x}}{\sqrt{K_{p,x}}}$$

$$K_{p,x} = \frac{\mu u_{\infty,x} \Delta x}{\Delta P}$$

, where $K_{p,x}$ is the Darcy permeability of brain tissue along *x*-axis.

The shear stresses along *y*- and *z*-axes can be calculated in a similar manner.

When the values listed in **A** are introduced in these equations, the magnitude of fluid shear stress is estimated as 0.86 - 3.9 Pa.

Table S1. Simulative Calculation of the Magnitude of PHM-Generated Fluid Shear Stress on the PFC Neurons, Related to Figure 2

(A) Values referenced for simulative calculation of the magnitude of fluid shear stress that PHM generated in the PFC. All referenced values except viscosity (marked with ♯) were drawn from analyses with ICP measurement and Gd-DTPA-enhanced MRI (Figures 2 and S5). The property of interstitial fluid viscosity was referenced from previous studies (Huang and Bonn, 2007; Sugiyama et al., 2013; Yao et al., 2013).

(B) Calculation of the magnitude of PHM-generated fluid shear stress. Fluid shear stress (τ) at the cell surface can be calculated as reported previously (Tarbell and Shi, 2013).

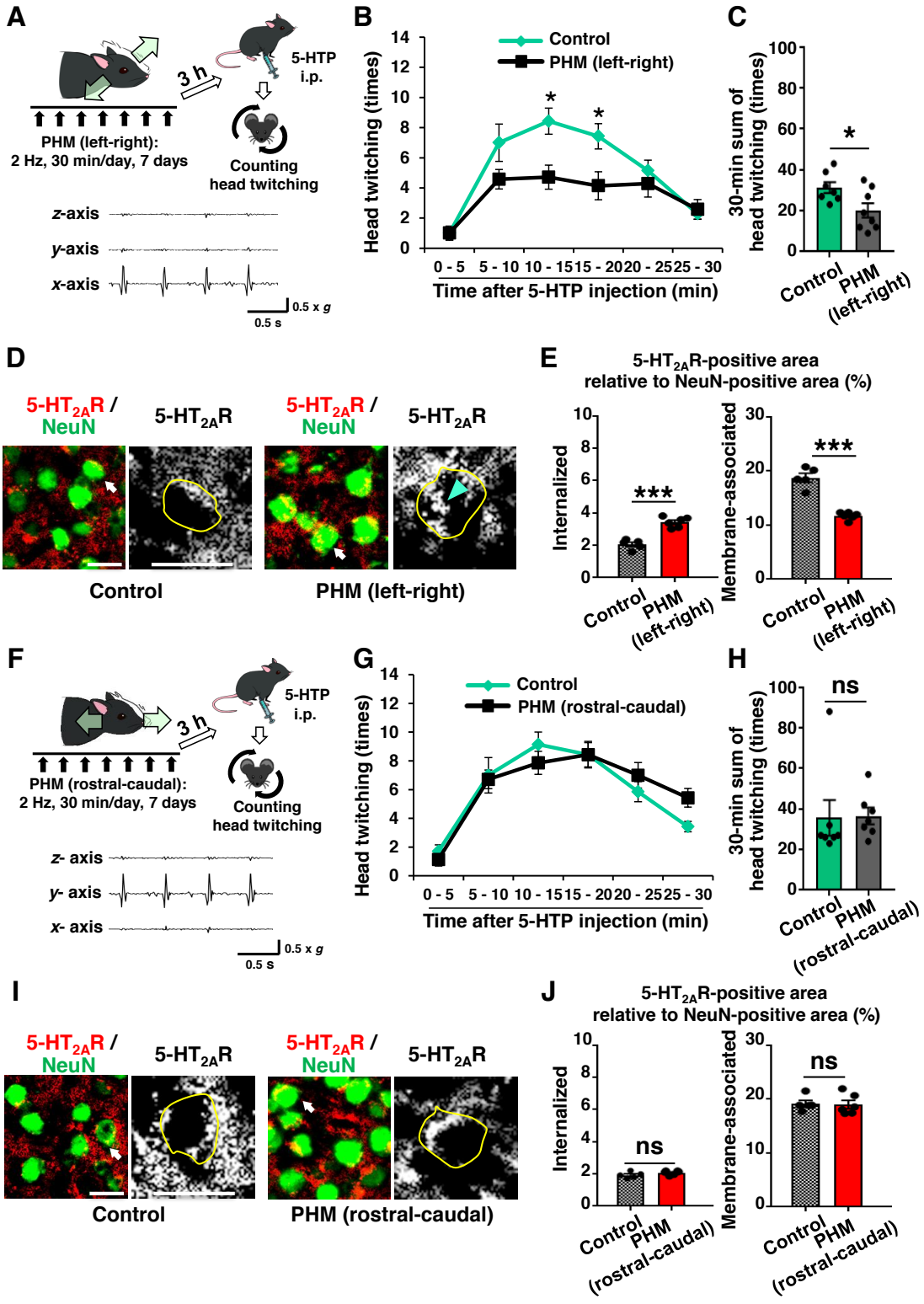

Figure S6. Effects of PHM in the Directions Other Than Vertical One, Related to Figure 2

(A-E) PHM in the left-right direction suppresses HTR and induces 5-HT_{2A} receptor internalization in PFC neurons of mice. (A, top) Schematic representation of experimental protocol for analysis of the effects of left-right PHM on HTR. 5-HTP administration for HTR test was conducted 3 h after the last bout of 1-week daily PHM. (A, bottom) The PHM system was adjusted to selectively produce 1.0 x *g* acceleration peaks along the *x*-axis. Accelerations of the rats' heads during PHM were measured as in Figure S1D, and presented following the definition of each axis shown in Figure S1C. Right-angled scale bar, 0.5 x *g* / 0.5 s. Images are representative of three independent experiments with similar results. (B-E) HTR and 5-HT_{2A} receptor internalization in PFC neurons of mice were analyzed as in Figures S3B-S3E (C, $p = 0.029$, unpaired t test; n = 7 mice for control group, n = 8 mice for PHM group) (E, internalized: $p < 0.001$, membrane-associated: $p < 0.001$, unpaired t test; n = 5 mice for control group, n = 6 mice for PHM group). Scale bars, 20 μm.

(F-J) PHM in the rostral-caudal direction neither suppresses HTR nor induces 5-HT_{2A} receptor internalization in PFC neurons of mice. (F, top) Schematic representation of experimental protocol for analysis of the effects of rostral-caudal PHM on HTR. 5-HTP administration for HTR test was conducted 3 h after the last bout of 1-week daily treadmill running. (F, bottom) The PHM system was adjusted to selectively produce 1.0 x *g* acceleration peaks along the *y*-axis. Accelerations at the rats' heads were measured and presented as in (A, bottom). (G-J) HTR and 5-HT_{2A} receptor internalization in PFC neurons of mice were analyzed as in Figures S3B-S3E (H, $p = 0.92$, unpaired t test; n = 7 mice for each group) (J, internalized: $p = 0.16$, membrane-associated: $p = 0.88$, unpaired t test; n = 5 mice for control group, n = 6 mice for PHM group). Scale bars, 20 μm.

Controls in (B-E and G-J) represent mice that were anesthetized, and placed in a prone position with their heads on the platform that was left static (30 min per day, 7 days). Data for the samples in (D, E, I and J) were obtained from mice infused with 4% PFA/PBS immediately after HTR test shown in (B, C, G and H). Data are represented as means ± SEM. $^{*}p < 0.05$; $^{***}p < 0.001$; ns, not significant. See also Figure S2.

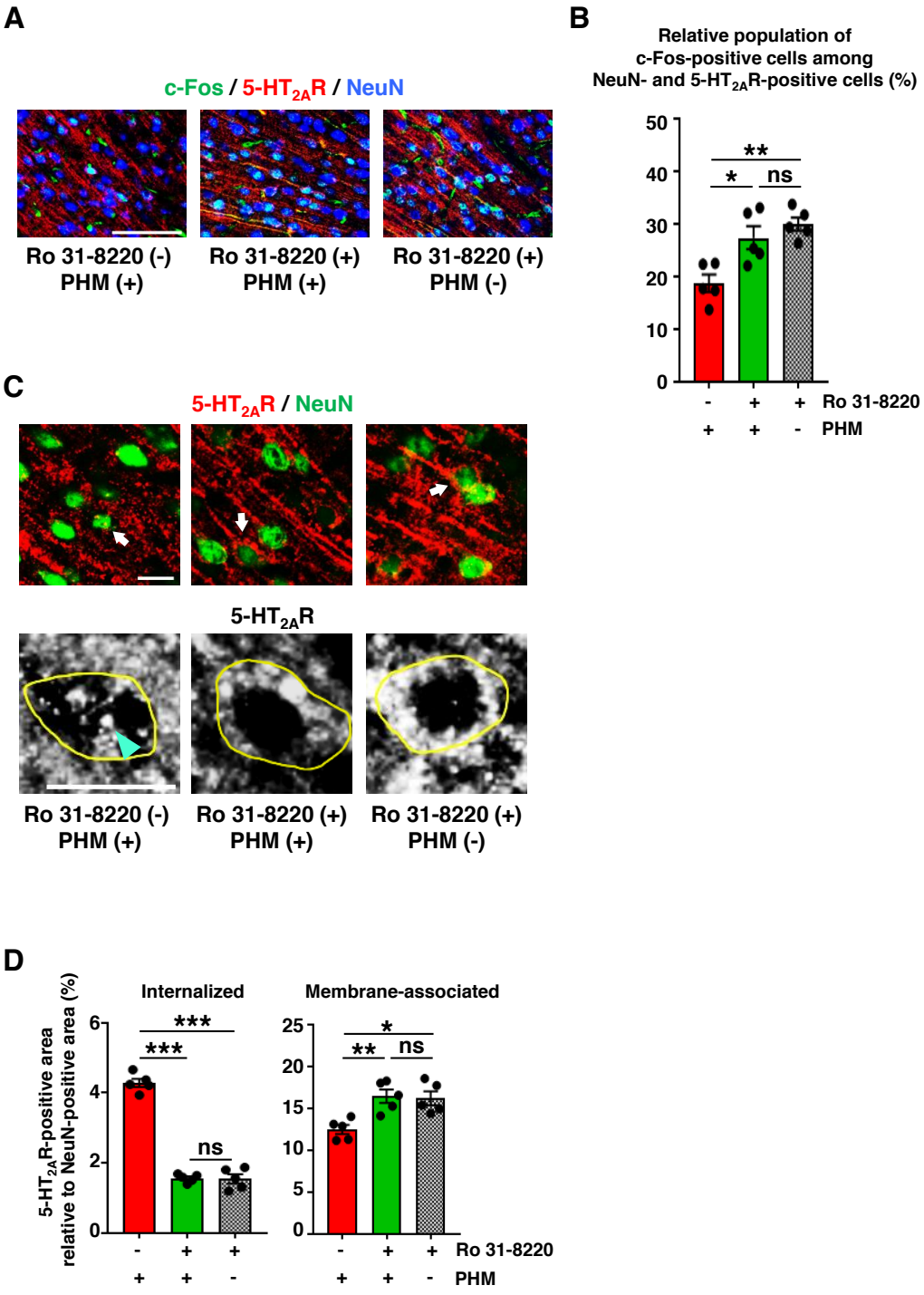

Figure S7. PKC Inhibition Eliminates the Effect of PHM on c-Fos Expression and 5-HT$_{2A}$ Receptor Internalization in Mouse PFC Neurons, Related to Figure 4

(A) Representative micrographic images of anti-c-Fos (green), anti-5-HT_{2A} receptor (red) and anti-NeuN (blue) immunostaining of the PFC of mice administered with Ro 31-8220 or its vehicle (saline) prior to each bout of daily PHM. Scale bar, 100 μm. Images are representative of five mice.

(B) PKC inhibition nullified the effect of PHM on c-Fos expression in 5-HT_{2A} receptor-positive neurons of the PFC of mice administered with 5-HTP. Relative population (%) of c-Fos-positive cells out of 300 NeuN- and 5-HT_{2A} receptor-positive cells is shown (column 1 vs. 2: $p = 0.013$, column 1 vs. 3: $p = 0.0020$, column 2 vs. 3: $p > 0.5$, one-way ANOVA with post hoc Bonferroni test; $n = 5$ mice for each group).

(C) Representative micrographic images of anti-5-HT_{2A} receptor (5-HT_{2A}R; red) and anti-NeuN (green) immunostaining of mouse PFC from each group. High magnification images of anti-5-HT_{2A} receptor immunostaining of arrow-pointed cells are presented with a gray scale. Yellow lines represent the margins of neuronal somas outlined by anti-NeuN immunosignals, and cyan arrowhead points to internalized anti-5-HT_{2A} receptor immunosignals. Scale bars, 20 μm. Images are representative of four to five mice.

(D) Internalized and membrane-associated 5-HT_{2A} receptor-positive areas were quantified as in Figure 1J. Thirty-five to forty NeuN-positive cells were analyzed for each mouse (left chart: $p < 0.001$ for column 1 vs. 2 and column 1 vs. 3, $p > 0.5$ for column 2 vs. 3. right chart: $p = 0.0076$ for column 1 vs. 2, $p = 0.012$ for column 1 vs. 3, $p > 0.5$ for column 2 vs. 3, one-way ANOVA with post hoc Bonferroni test; $n = 5$ mice for each group). Data for (A-D) were obtained from mice infused with 4% PFA/PBS immediately after HTR test shown in Figures 4F and 4G.

Data are represented as means ± SEM. $^{*}p < 0.05$, $^{**}p < 0.01$, $^{***}p < 0.001$; ns, not significant. See also Figure S2.

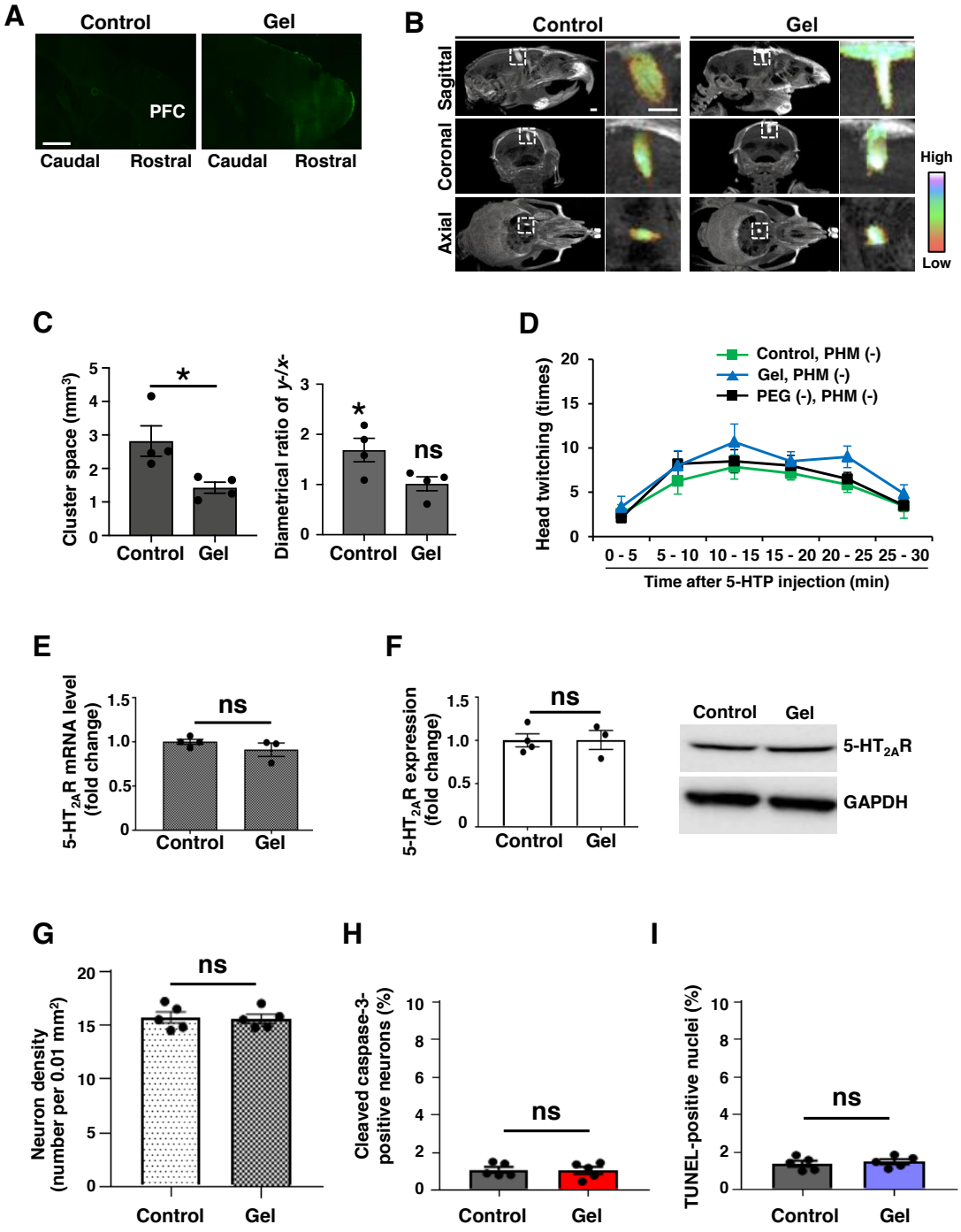

Figure S8. Hydrogel Introduction Hinders Interstitial Fluid Movement, but Does not Delay HTR after 5-HTP Injection, Alter 5-HT$_{2A}$ Receptor Expression, or Affect Neuronal Survival/Apoptosis, Related to Figure 5

(A) Introduction of PEG hydrogel in mouse PFC. Twenty-four hours after the injection of pre-gel fluorescent PEG solution or its ungelatable control, PFC samples

were prepared. Scale bar, 1 mm. Representative sagittal images from three or four mice for each group are shown.

(B) Injected contrast medium does not enter mouse PFC after hydrogel introduction. Three hours after the injection of pre-gel PEG solution or its ungelatable control, iodine-based contrast medium (Isovist) was microinjected into the PFC. Contrast medium was visualized by μCT imaging. (B) Sagittal, coronal, and axial μCT images of Isovist-injected mouse PFC, with or without hydrogel introduction. Isovist-derived signal intensity is presented as pseudo-color in high magnification images (right) that refer to the areas indicated by dotted rectangles in low magnification images (left). Scale bars, 1 mm. Note that injected Isovist appears to remain where the needles were inserted or flow back to the brain surface without substantially entering the interstitial space of the PFC.

(C) Quantification of Isovist clusters remaining in the PFC. Isovist cluster ≥500 μm away from the brain surface were quantified for their occupying spaces (left chart, $p = 0.0278$, unpaired t test; n = 4 mice for each group) and diametrical ratios of *y*- (rostral-caudal) to *x*- (left-right) axis (right chart, $p = 0.026$ and 0.92 for columns 1 and 2, respectively related to the statistical hypothesis that the ratio is 1, unpaired t test; n = 4 mice for each group). Consistent with the anisotropic enhancement of interstitial fluid movement by PHM (Figures 2G and 2H), Isovist clusters dominantly spread along *y*-axis rather than *x*-axis in control mouse PFC (right chart).

(D) Hydrogel introduction does not delay HTR after 5-HTP administration. Data shown as ‘Control, 1st HTR’ and ‘Gel, 1st HTR’ in Figure 5B are merged with those shown as ‘Control 1’ in Figure 1B. Green and blue lines correspond to the green and blue lines in Figure 5B, respectively, and black line correspond to the black line in Figure 1B.

(E and F) Hydrogel introduction does not alter 5-HT_{2A} receptor expression in mouse PFC. Two weeks after the injection of pre-gel or its control PEG solution, mRNA (E) and protein (F) expression of 5-HT_{2A} receptor in mouse PFC were quantitatively analyzed as in Figures S2E and S2F. The mean values of control samples (column 1 or lane 1 in each panel) were set as 1 (E: $p = 0.97$, F: $p = 0.27$, unpaired t test; $n = 4$ mice for control group, $n = 3$ mice for Gel group).

(G-I) Hydrogel introduction does not affect neuronal survival/apoptosis or overall cell apoptosis. Mouse PFC sections prepared for Figure 5D were subjected to anti-NeuN and anti-cleaved caspase-3 immunostaining (G and H) or TUNEL assay (I). NeuN-positive neuronal somas were counted (G), and the ratios of NeuN- and cleaved caspase-3-double positive somas among them (H) and TUNEL-positive nuclei (I) were quantified. Each value represents an average from 5 images of 500 x 500-μm area analyzed for each mouse (G: $p = 0.85$, H: $p = 0.88$, I: $p = 0.64$, unpaired t test; $n = 5$ mice for each group).

Data are represented as means ± SEM. $^{*}p < 0.05$; ns, not significant.

Transparent Methods

Animal experiments

Animals were housed under a 12 h/12 h light/dark cycle with controlled temperature (23 - 25°C), and treated with humane care under approval from the Animal Care and Use Committee of National Rehabilitation Center for Persons with Disabilities and Tokyo Metropolitan Institute of Gerontology. Male C57BL/6 mice and Sprague-Dawley (SD) rats were purchased from Charles River (Yokohama, Japan) or SLC (Hamamatsu, Japan), acclimated to the laboratory environments for at least 1 week, randomly divided into experimental groups, and used for experiments at the age of 9 - 10 weeks (mice) and 8 - 9 weeks (rats). All the animal behavior tests were conducted between 4 pm and 8 pm. We made every effort to relieve suffers of animals during experiments and to minimize the number of animals.

Chemicals, plasmids and antibodies

All the chemicals were purchased from Sigma-Aldrich unless noted otherwise. The pcDNA 3.1-based expression vector plasmid for human 5-HT_{2A} receptor was purchased from transOMIC Technologies (Huntsville, AL). The pcDNA3-based expression vector for mCherry was obtained from the shared resources of Mechanobiology Institute in National University of Singapore. Antibodies used in this study are described in the KEY RESOURCES TABLE.

Treadmill running, PHM and acceleration analysis

As an animal model of physical exercise, mice were subjected to compulsive running using a belt drive treadmill equipped with an electrical shock system (MK-680S, Muromachi, Tokyo, Japan). We habituated the animals of both control and running groups to the treadmill system by placing them in the machine several times without

turning on the treadmill belt during the acclimation period. The electrical stimulation was turned on only once or twice during the first 5 minutes of the 30-minute treadmill running on the first day of the 1-week treadmill running period. Thereafter, we did not need to turn on the electrical shock system to have the animals keep running, perhaps because the velocities we employed (10 m/min for mice, and 20 m/min for rats) were moderate. The control mice in treadmill running experiments were placed on the belt for a defined period of time without turning on the treadmilling.

Animals (mice or rats) were subjected to PHM in a prone position using a platform that we developed to move their heads (schematically represented in Figures 1D, 2A, 2E, 4E, 5A, S4A, S4F, S6A, and S6F). During PHM, animals were kept anesthetized with 1.2% isoflurane except for the MRI study, in which we used the combination of midazolam, butorphanol and medetomidine for anesthesia. Body temperature of tested animals was maintained using a light heater. The control mice in PHM experiments were anesthetized likewise, and placed in a prone position with their heads on the platform that was left static.

To measure the accelerations at the head during treadmill running or PHM, we fixed an accelerometer (NinjaScan-Light; Switchscience, Tokyo, Japan) on the rats' heads with a surgical tape. Acceleration-specific signals were extracted and average accelerations for 3-D (*x*-, *y*- and *z*-axes) were individually calculated from 10 serial waves using the software applications provided from the manufacture and Spike2 (CED, Cambridge, UK). The PHM system was set up to produce 1.0 x *g* vertical acceleration peaks at the head of rodents examined.

Head-twitch response (HTR) test

After administration of 5-HTP (100 mg/kg) or its vehicle (normal saline) by i.p., mice were individually placed in a Plexiglas box and videotaped for 30 min using a video

camera (HDR-CX700, Sony, Tokyo, Japan). Recorded movies were reviewed to count head twitching. 5-HTP was injected 3 h after the last bout of treadmill running or PHM.

Measurement of intracerebral pressure (ICP) at rats' PFC

ICP was measured using a blood pressure telemeter (Millar, Houston, TX) with its sensor placed in rats' PFC. During ICP measurement, respiration was monitored using a respiration sensor attached to the tested rats. Low-pass (50 Hz) filtered ICP waves were analyzed using LabChart 8 (ADInstruments, Dunedin, New Zealand) software. We observed ~0.5-Hz respiration-synchronized ICP changes with ~2.5 mm Hg magnitude (peak to peak) as well as 2-Hz PHM-specific waves with ~1 mm Hg magnitude (peak to peak) (Figures 2B-2D).

In vivo analysis of the distribution dynamics of cerebral interstitial fluid using MRI

MRI Scanning: 8-week-old male SD rats were scanned in an ICON 1.0-Tesla bench top MRI system (Bruker BioSpin, Esslingen, Germany) using a T1-weighted-fast low angle shot-navigation-highers-three-dimensional (T1-FLASH-nav-highers-3-D) sequence. Parameters for the T1-FLASH-nav-highers-3-D sequence were as follows; echo time (TE): 12.0 ms, repetition time (TR): 50.0 ms, flip angle (FA): 30°, slice thickness (SL): 0.84 mm, field of view (FOV): 35 × 35 × 27 mm, voxel: 0.137 × 0.137 × 0.84 mm^3. Each scanning took 10 min.

Intracerebral microinjection of Gd-DTPA solution: Rats were first subjected to brain pre-scanning with MRI under isoflurane anesthesia, and then to intracerebral microinjection of Gd-DTPA (Magnevist®, Bayer, Leverkusen, Germany) as previously reported with some modifications. In brief, a 31-G microsyringe (Hamilton Bonaduz AG, Bonaduz, Switzerland) was stereotaxically positioned on rats

anesthetized with 2 mg/kg of midazolam (Sandoz, Basel, Switzerland), 2.5 mg/kg of butorphanol (Meiji Seika, Tokyo, Japan) and 0.15 mg/kg of medetomidine (Kyoritsu Seiyaku, Tokyo, Japan), such that 1 μl of Gd-DTPA solution (diluted to 25 mM with normal saline) could be infused with the rate fixed at 0.2 μl/min using a microsyringe pump instrument (KD scientific, Holliston, MA). The needle placement measurements were as follows; anterior: 2.5 - 3.0 mm, lateral: 1.5 - 2.0 mm, ventral: 2.0 - 3.0 mm from the bregma. After the injection, we held the microsyringe for 5 min to avoid reflux, pulled out the needle carefully, and sutured the skin.

MRI data acquisition and post-processing: Following intraparenchymal Gd-DTPA injection, rats were subjected to two serial brain MRI scans between which PHM was either applied or left unapplied (kept sedentary) for 30 min (Figure 2E). MR images were analyzed using a software package rSPM (Gaser et al., 2012), which is a modified version of SPM12 (http://www.fil.ion.ucl.ac.uk/spm/software/spm12/) developed for human neuroimaging data analyses. The original data were converted from the DICOM format to the NIfTI format. Each individual rat brain image was realigned to the first volume and spatially normalized to a template brain image provided by rSPM. The normalized data had an 86 x 121 x 66 matrix with a 0.2 x 0.2 x 0.2 mm^3 isotropic voxel. The Gd-DTPA cluster was defined as voxels with top 0.05% signal intensity in each volume.

Simulative calculation of the magnitude of fluid shear stress on the PFC neurons during PHM

Interstitial fluid flow in the brain tissue follows the Henry Darcy's law, which defines the flux density of penetrating fluid per unite time. The velocity of interstitial fluid flow (u) is assumed to approach the superficial velocity (u_∞) and zero ($u = 0$) at the cell surface (i.e. a no-slip condition). Using these two boundary conditions together

with the Brinkman equation, fluid shear stress (τ) at the interstitial cell surface can be obtained as described in Table S1.

Neuronal cell culture and plasmid transfection

Mouse neuroblastoma-derived Neuro2A cells (provided from Dr. Yokota, Tokyo Medical and Dental University, Japan), which exhibit neuronal phenotypes and morphology (Goshima et al., 1993; Yun et al., 2013), were cultured in DMEM (Wako, Osaka, Japan) with 10% fetal bovine serum (FBS; GE Healthcare Life Science Marlborough, MA) at 37°C in a 5% CO_2 incubator. At approximately 70% confluence in a 10-cm culture dish (Corning Life Sciences, Corning, NY), Neuro2A cells were transfected with 10 μg of a 5-HT_{2A} receptor expression vector plasmid using lipofectamine® 3000 (Thermo Fisher Scientific, Waltham, MA) according to the manufacturer's directions. Neuro2A is not a commonly misidentified cell line maintained by ICLAC. We confirmed the expression of neuronal proteins such as TUJ-1 (neuron-specific Class III β-tubulin) and the axonal formation. The cell line was not tested for mycoplasma contamination. However, when we conducted DAPI staining, we did not observe a dotted stain around the nuclei, which is characteristic of mycoplasma contamination.

Application of FSS to neuronal cells in culture

Neuro2A cells grown in a poly-D-lysine coated 35-mm culture dish (Corning Life Sciences) were cultured in serum-free DMEM for 24 h before exposure to FSS (0.91 Pa) for 30 min. As we previously reported (Yoshino et al., 2013), a parallel plate flow-chamber and roller pump (Masterflex, Cole-Parmer, IL) were used to apply FSS. The flow-chamber, which was composed of a cell culture dish, a polycarbonate I/O unit, and a silicone gasket, generated a 23-mm-long 10-mm-wide 0.5-mm-high flow channel. The flow circuit was filled with serum-free medium. To maintain pH and

temperature of culture medium, we used a 5% CO_2-containing reservoir and a temperature-controlled bath.

Live cell imaging to monitor intracellular calcium (Ca^{2+}) concentration

We conducted live cell imaging to monitor intracellular Ca^{2+} concentration after 5-HT administration. Neuro2A cells grown in a 10-cm dish were transfected with 10 μg of 5-HT_{2A} receptor and 5 μg of mCherry expression plasmid vector using lipofectamine® 3000 (Thermo Fisher Scientific). Forty-eight hours after transfection, cells were transferred and grown overnight in a poly-D-lysine coated 35-mm dish, which was placed in a 37ºC/5%-CO_2 plate type incubator (Tokai Hit, Fujinomiya, Japan) attached to a microscope (BZ-9000 HS, Keyence, Osaka, Japan). Then, a flow chamber was set to the dish plate and FSS was applied. Cells, either left unexposed or exposed to FSS (average 0.91 Pa, 30 min), were loaded with Fluo 4-AM dye (DOJINDO, Kumamoto, Japan) for 60 min in a 37ºC/5%-CO_2 incubator. Cells were then placed on an incubator-attached fluorescence microscope, and treated with 5-HT (10 μM). Ten minutes after 5-HT administration, green fluorescence emitted from Fluo 4-AM bound to Ca^{2+} was viewed with the microscope.

Immunohistochemical analysis of mouse PFC

After the completion of HTR tests, animals were anesthetized by administrating combinations of midazolam, butorphanol and medetomidine, and perfused with 4% PFA in phosphate-buffered saline (PBS) transcardially. Then, brains were excised, post-fixed in 4% PFA in PBS for additional 24 h at 4ºC, and stored in 30% sucrose/PBS until they sank. Fixed brains were frozen in OCT (Sakura Finetek, Tokyo, Japan) and cut into 20 μm-thick sagittal sections using a cryostat (CM3050S, Leica Microsystems, Wetzlar, Germany). Sliced sections were permeabilized with 0.1% Tween-20 in Tris-buffered saline, blocked with 4% donkey serum (Merck

Millipore, Burlington, MA), stained by incubating with primary antibodies at appropriate concentrations followed by their species-matched secondary antibodies conjugated with Alexa Fluor 488, 568 or 645 (Thermo Fisher Scientific), and viewed with a fluorescence microscope (BZ-9000 HS, Keyence).

Immunocytochemical analysis of Neuro2A cells

Neuro2A cells grown in a poly-D-lysine-coated dish were washed once with ice-cold PBS, fixed with 4% PFA in PBS, permeabilized with 0.1% Triton X-100 in PBS, incubated with a blocking solution (10% FBS, Thermo Fisher Scientific), and stained using target-specific primary and their species-matched secondary antibodies. DAPI was used for nuclear staining. Cells were then viewed with a fluorescence microscope (BZ-9000 HS, Keyence).

Quantitative analysis of 5-HT_{2A} receptor internalization in vivo and in vitro

To quantify 5-HT_{2A} receptor internalization in PFC neurons, we defined 'internalized' and 'membrane-associated' 5-HT_{2A} receptor-positive signals based on the distance from soma outlines and the connectivity with marginal regions. We outlined the somas of individual PFC neurons by tracing the outlines of NeuN-positive area (see yellow lines in Figure S2B). The anti-5-HT_{2A} receptor immunosignals that appeared along the marginal outlines were mostly distributed within 2 μm of soma margins (Figure S2A). In the case of Neuro2A cells, we outlined their soma margins by anti-TUJ-1 (neuron-specific Class III β -tubulin) immunostaining, because anti-NeuN immunosignals did not clearly indicate them. Immunostaining of 5-HT_{2A} receptor-expressing Neuro2A cells grown in a poly-D-lysine-coated culture dish revealed that the major portion of 5-HT_{2A} receptor distribution was along the soma margins with its peak <2 μm away from their outlines (Figure S2C). In contrast, treatment of Neuro2A cells with 5-HT (10 μM, 15 min), which is known to induce 5-HT receptor

internalization (Baldys and Raymond, 2011; Bhattacharyya et al., 2002), altered the distributional profile of the anti-5-HT_{2A} receptor immunosignal intensity, shifting its peak >2 μm away from soma outlines (Figure S2C). Based on these observations, we defined the anti-5-HT_{2A} receptor immunosignals within 2 μm of soma outlines as 'membrane-associated' (Figures S2B and S2D). Resultantly, the anti-5-HT_{2A} receptor immunosignals distributed at >2 μm from soma outlines were defined as 'internalized' (Figures S2B and S2D). In the case of in vivo analysis (i.e. immunostaining of mouse PFC), anti-5-HT_{2A} receptor immunosignals connected with perimarginal regions were defines as 'membrane-associated', regardless of the distance from soma outlines. To avoid the possible underestimation of membrane-associated area for images in which 'peripheral' parts of cells were scanned, somas larger than 10 μm in short diameter were subjected to the quantification of 5-HT_{2A} receptor internalization. Images were analyzed using Photoshop CC (Adobe Systems, San Jose, CA) and ImageJ (NIH, Bethesda, MD) software.

We quantified 5-HT_{2A} receptor-internalization based on the ratio of internalized or membrane-associated anti-5-HT_{2A} receptor immunosignal-positive area to total soma area defined by outlining anti-NeuN (mouse PFC neurons) or anti-TUJ-1 (Neuro2A cells) immunosignal-positive area (Figures 1J, 3C, 4D, 5E, S3E, S3J, S4E, S4J, S6E, S6J, and S7D). Images were analyzed using BZ-H1C (BZ-9000 HS related application, Keyence), Photoshop CC and ImageJ software.

Quantitative PCR analysis (reverse transcription and real-time PCR)

Five hundred nanograms of total RNA extracted from mouse PFC excised immediately after cervical dislocation were subjected to reverse transcription, using ISOGEN II (NIPPON GENE, Tokyo, Japan) and PrimeScript® RT reagent Kit (TaKaRa, Kusatsu, Japan). The resulting cDNA was subjected to real-time PCR

analysis using glyceraldehyde-3-phosphate dehydrogenase (GAPDH) as an internal control in Applied Biosystems 7500 Real Time PCR System with Power SYBR Green PCR Master Mix (Thermo Fisher Scientific).

The primers (sense and antisense, respectively) were as follows: mouse *Htr2a*, 5'-TGCCGTCTGGATTTACCTGG-3' and 5'-TGGTTCTGGAGTTGAAGCGG-3', mouse *Gapdh*, 5'-GCAAAGTGGAGATTGTTGCCAT-3' and 5'- CCTTGACTGTGCCGTTGAATTT -3'.

Immunoblot analysis

Mouse PFC tissue was excised immediately after cervical dislocation, mechanically homogenized, solubilized with sodium dodecyl sulfate (SDS) sample buffer (50 mM Tris-HCl pH 7.0, 18% glycerol, 2% SDS), and subjected to SDS-PAGE followed by anti-5-HT_{2A} receptor and anti-GADPH immunoblotting. Specific signals were visualized and quantified using Odyssey infrared imaging system (LI-COR Biosciences, Lincoln, NE) and ImageJ software.

Hindrance of interstitial fluid movement (flow) by introduction of hydrogel in mouse PFC

Preparation of a pre-mixed solution of polyethylene glycol (PEG) with functional groups: Equal volume of tetra-armed thiol-terminal (TetraPEG-SH) (Yuka-Sangyo, Tokyo, Japan) and acrylate-terminal (Tetra-PEG-ACR) (JenKem Technology, Plano, TX) PEG solutions (25 g/L in PBS) were mixed just before use (Hayashi et al., 2017). Tetra-armed polyethylene glycol without functional groups (25 g/L in PBS) was used as an ungelatable control. For the analysis of hydrogel distribution in the mouse PFC, we used Tetra-PEG-SH fluorescently labeled with a thiol-reactive probe (Merck KGaA, Darmstadt, Germany).

Intracerebral microinjection of PEG solution: A 31-G syringe (Terumo Corporation, Tokyo, Japan) was stereotaxically positioned on mice anesthetized with intraperitoneal injection of a mixture of three anesthetic agents (midazolam, butorphanol, medetomidine), such that 4 μl of pre-mixed PEG solution could be injected with the rate fixed at 0.2 μl/min using a microsyringe pump. The needle placement measurements were as follows; anterior: 1.5 - 2.0 mm, lateral: 1.5 - 2.0 mm, ventral: 1.0 - 1.5 mm from the bregma. After the injection, we held the syringe for 5 min to avoid reflux, pulled out the needle carefully, and sutured the skin.

To dissect the effects of PHM on HTR from those resulting from these experimental procedures, we gave 1-week recovery time before the first HTR test and subsequent PHM application to the mice (daily 30 min, 7 days). Three hours after the last bout of PHM, the second HTR test was conducted (see Figure 5A). Immediately following 30-min counting of head twitching after 5-HTP administration, mice were sacrificed by transcardial infusion of paraformaldehyde and subjected to histological analysis.

μCT analysis of the effect of hydrogel introduction in mouse PFC

Three hours after the injection of either the pre-gel PEG solution or its ungelatable control, 5 μl of an iodine-based contrast medium (Isovist® inj. 300, Bayer) was microinjected and visualized using μCT (inspeXio SMX-100CT, Shimadzu, Kyoto, Japan). Although contrast medium injection was conducted separately from PEG injection (i.e., the needle was pulled out and the skin was sutured once PEG infusion was completed), the stereotaxic needle placement position was identical between PEG and contrast medium injections. The rate of contrast medium infusion was fixed at 0.5 μl/min. After the injection, we held the microsyringe for 5 min to avoid reflux, pulled out the needle carefully, and sutured the skin. μCT images were obtained with

following parameters; voxel size 50 μm, 60 KeV, 58 μA, field of view 25.6 mm, matrix size 512 x 512. 3D reconstructed objects were visualized and analyzed on software for 3D morphometry (TRI/3D-BON-FCS64, RATOC System, Tokyo, Japan). The contrast medium cluster in mouse PFC was defined as voxels with ≥1.3 times signal intensity as compared to that of air.

Terminal deoxynucleotidyl transferase-mediated dUTP nick-end labeling (TUNEL) assay

Mouse PFC sections were stained using a TUNEL kit (Biotium, Fremont, CA) according to the manufacturer's protocols, counterstained with DAPI, and then viewed using a 20x objective with a fluorescence microscope (BZ-9000 HS, Keyence). The nuclei of apoptotic cells were determined by the existence of green fluorescent patches, and cell apoptosis was quantified by referring their counts to total nuclear numbers defined by DAPI staining.

Statistical analysis

All the quantitative data are presented as means ± SEM. Parametric statistical analyses were conducted by two-tailed t test for two-group comparison and ANOVA with post hoc (Bonferroni or Dunnett) for multiple (≥ 3) group comparison, using SPSS (Version 24, IBM SPSS, Chicago, IL) and PRISM (version 7, GraphPad Software, San Diego, CA). Differences were considered as significant at p values below 0.05.

Adequate sample sizes of experiments were estimated based on our pilot experiments and experience with similar measurements to ensure adequate power to detect a specified effect size. For animal behavioral analyses, at least 4 animals were assigned to each experimental group according to standard scientific conventions. We tried to reach a conclusion for each individual experiment using the smallest sample

size possible. No data were excluded except for MRI analysis, from which data from a rat with unsuccessful microinjection of Gd-DTPA were eliminated. The investigators were not blinded to any group allocations for in vivo or in vitro experiments.

KEY RESOURCES TABLE

REAGENT or RESOURCE	SOURCE	IDENTIFIER
Antibodies		
Mouse monoclonal anti-NeuN (clone A60)	EMD Millipore (Merck)	RRID:AB_2298772 Catalog# MAB377
Rabbit monoclonal anti-phospho-p44/42 MAPK	Cell Signaling Technology	RRID:AB_2315112 Catalog# 4370
Rabbit monoclonal anti-GAPDH	Cell Signaling Technology	RRID:AB_10622025 Catalog# 5174
Mouse monoclonal anti-β-III tubulin	Abcam	RRID:AB_2256751 Catalog# ab78078
Rabbit polyclonal anti-β-III tubulin	Abcam	RRID:AB_444319 Catalog# ab18207
Rabbit polyclonal anti-phospho-MARCKS	Sigma-Aldrich	Catalog# P0370
Mouse monoclonal anti-5-HT_{2A} receptor	Santa Cruz Biotechnology	Catalog# sc-166775
Goat polyclonal anti-5-HT_{2A} receptor	Santa Cruz Biotechnology	Catalog# sc-15073
Rabbit polyclonal anti-c-Fos	Santa Cruz Biotechnology	RRID:AB_2106783 Catalog# sc-52
Rabbit polyclonal anti-PKCγ	Santa Cruz Biotechnology	RRID:AB_632234 Catalog# sc-211
Rabbit polyclonal anti-cleaved Caspase-3 (Asp175)	Cell Signaling Technology	Catalog# 9661L
Bacterial and Virus Strains		
N/A		
Biological Samples		
N/A		
Chemicals, Peptides, and Recombinant Proteins		
Lipofectamine 3000	Thermo Fisher Scientific	Catalog# L300008
Tetra-PEG-SH	Yuka-Sangyo	SUNBRIGHT PTE-200SH
Tetra-PEG-ACR	JenKem Technology	4ARM-ACLT-20K
Tetra-PEG-SH fluorescently labeled with a thiol-reactive probe	Merck KGaA	Catalog# 595504
4ARM-PEG (ungelatable PEG solution)	JenKem Technology	MW 20K
5-hydroxytryptophan (5-HTP)	Sigma-Aldrich	Catalog# H9772
Serotonin (5-HT)	Sigma-Aldrich	Catalog# H9523
Ro 31-8220 (PKC inhibitor)	Sigma-Aldrich	Catalog# R136
Magnevist (contrast agent for MRI)	Bayer	Catalog# 341108168
Isovist (contrast agent for CT)	Bayer	Catalog# 877219
Critical Commercial Assays		
PrimeScript RT reagent Kit (reverse transcription kit)	TaKaRa	Catalog# RR037A
ISOGEN II (reagent for RNA extraction)	NIPPON GENE	Catalog# 311-07361
SYBR Green Master Mix (reagent mix for qPCR)	Thermo Fisher Scientific	Catalog# 4368706
Fluo 4-AM (fluorescent Ca^{2+} probe)	DOJINDO	Product code F311
TUNEL Assay Apoptosis Detection Kit	Biotium	Catalog# 30074
Deposited Data		

N/A		
Experimental Models: Cell Lines		
Neuro2A cells	Mouse neuroblastoma	N/A
Experimental Models: Organisms/Strains		
N/A		
Oligonucleotides		
Mouse HT_{2A} receptor: 5'-TGCCGTCTGGATTTACCTGG-3' and 5'-TGGTTCTGGAGTTGAAGCGG-3'		
Mouse GAPDH: 5'-GCAAAGTGGAGATTGTTGCCAT-3' and 5'-CCTTGACTGTGCCGTTGAATTT-3'		
Recombinant DNA		
Expression vector for mCherry (pcDNA3-mCherry)	National University of Singapore.	N/A
Expression vector for human 5-HT_{2A} receptor (pcDNA3.1-5-HT_{2A} receptor)	transOMIC Technologies	N/A
Software and Algorithms		
TRI/3D-BON, TRI/3D-BON-C	RATOC Systems	N/A
ImageJ	NIH	N/A
SPSS	IBM SPSS	Version 24
PRISM	GraphPad Software	Version 7
Other		

Supplemental References

Baldys, A., and Raymond, J.R. (2011). Role of c-Cbl carboxyl terminus in serotonin 5-HT_{2A} receptor recycling and resensitization. J. Biol. Chem. *286*, 24656-24665.

Gaser, C., Schmidt, S., Metzler, M., Herrmann, K.H., Krumbein, I., Reichenbach, J.R., and Witte, O.W. (2012). Deformation-based brain morphometry in rats. Neuroimage *63*, 47-53.

Huang, N., and Bonn, D. (2007). Viscosity of a dense suspension in Couette flow. J. Fluid Mech. *590*, 497-507.

Sugiyama, S., Saito, R., Funamoto, K., Nakayama, T., Sonoda, Y., Yamashita, Y., Inoue, T., Kumabe, T., Hayase, T., and Tominaga, T. (2013). Computational simulation of convection-enhanced drug delivery in the non-human primate brainstem: a simple model predicting the drug distribution. Neurol. Res. *35*, 773-781.

Tarbell, J.M., and Shi, Z.-D. (2013). Effect of the glycocalyx layer on transmission of interstitial flow shear stress to embedded cells. Biomech. Model Mechanobiol. *12*, 111–121.

Yao, W., Shen, Z., and Ding, G. (2013). Simulation of interstitial fluid flow in ligaments: comparison among Stokes, Brinkman and Darcy models. Int. J. Biol. Sci. *9*, 1050-1056.